Available online at www.sciencedirect.com
ScienceDirect
Coordination Chemistry Reviews 253 (2009) 37–55
COORDINATION CHEMISTRY REVIEWS
www.elsevier.com/locate/ccr

Review

Transition metal–σ-borane complexes

Krishna K. Pandey *

School of Chemical Sciences, Devi Ahilya University Indore, Khandwa Road campus, Indore 452 017, India

Received 4 September 2007; accepted 28 November 2007
Available online 3 December 2007

Contents

1. Introduction 38
2. Synthesis of metal–σ-borane complexes 38
   2.1. Titanium complexes 38
   2.2. Manganese and rhenium complexes 38
   2.3. Ruthenium complexes 39
   2.4. Nickel complexes 39
3. Elongated metal–σ-borane complexes 40
4. Reactivity of metal–σ-borane complexes 40
5. Spectroscopic studies 40
6. X-ray crystal structural studies 40
7. Theoretical studies 41
   7.1. Theoretical methods 42
   7.2. Bonding in titanium–σ-borane complexes 42
   7.3. Bonding in manganese–σ-borane complexes 43
   7.4. Bonding in rhenium–σ-borane complexes 45
   7.5. Bonding in ruthenium–σ-borane complexes 47
   7.6. Bonding in nickel, palladium and platinum–σ-borane complexes 47
   7.7. Bonding in rhodium–σ-borane complexes 52
   7.8. Bonding in intermediate iron and tungsten–σ-borane complexes 53
8. Conclusion 54
   Acknowledgement 54
   References 54

Abstract

Synthesis, structure and bonding in transition metal complexes with borane ligands HBcat' (catecholborane or substituted catecholborane), HBpin (pinacolborane), $HBCy_2$ (dicyclohexylborane), $HBEt_2$ (diethylborane) and $HBMe_2$ (dimethylborane) have been discussed. The review summarizes the results and progress in the understanding of the nature of the metal–borane bonds, which has been gained in recent theoretical studies. Geometrical data (both experimental and theoretically calculated) show M–B, M–H and B–H bond distances longer than the sum of covalent radii. These results are consistent with the interaction of both boron and hydrogen with metal central, while preserving B–H bond character. The nature of the metal–borane interactions is quantitatively analyzed with an energy decomposition analysis. The $[L_nM]$-$[\eta^2$-$BHR_2]$ bonding in metal–borane complexes is more than half electrostatic.

Keywords: Transition metal; Borane complexes; Structure; Spectroscopy; Chemical bonding

* Tel.: +91 731 2460208; fax: +91 731 2365782.
E-mail address: k_k_pandey3@rediffmail.com.

0010-8545/$ – see front matter © 2007 Elsevier B.V. All rights reserved.
doi:10.1016/j.ccr.2007.11.026

1. Introduction

A σ-complex is defined as the coordination of an H-E (E = H, B, C, Si) bond to a metal center, a two electron three center bond. Transition metal σ-complexes have attracted much attention due to their role in the oxidative addition and reductive elimination steps occurring in a wide variety of catalytic processes [1]. Since the report of the first σ-dihydrogen complex [2] in 1984, numerous examples of σ-dihydrogen [3–11] and σ-silane [12–20] complexes have been synthesized and characterized. In contrast to the large number of dihydrogen and σ-silane complexes, relatively few stable σ-borane [21–29] have been reported. Synthesis and bonding of the transition metal complexes containing residual B···H interaction have been reported [30–38]. Mechanistic studies have revealed that σ-borane complexes can be intermediates in catalytic hydroboration processes [32,39–41]. The reactions of transition metal complexes with boranes, in particularly, HBpin and HBcat (pin = 1,2-$O_2C_2Me_4$, cat = 1,2-$O_2C_6H_4$) involve either B–H oxidative addition to give hydride boryl complexes [42,43] or formation of σ-borane complexes. B–H oxidative addition can be implicated in catalytic hydroboration and dehydrogenative borylation of alkenes [44–46]. The formation and properties of metal boryl complexes, key intermediates in all of these reactions have been reviewed [47–54]. Photochemical B–H oxidative addition was first reported by Hartwig and He [55,56]. Perutz and co-workers reported photoinduced B–H oxidative addition of HBpin at $[Ru(depe)_2H_2]$ and $[Rh(triphos)H_3]$ [57]. Recently, Perutz and Sabo-Etienne investigated hydroboration and dehydrogenative borylation of alkenes using $[RuH\{(\mu\text{-}H)_2Bpin\}(\sigma\text{-}HBpin)(PCy_3)_2]$ [58] A review, dealing with σ-complex-assisted metathesis mechanismn in catalysis, has been written by Caballero and Sabo-Etienne [59]. The catalytic hydroboration and dehydrogenative borylation of alkenes reactions are not examined here. In this review, synthesis, reactivity, structure bonding in σ-borane complexes will be discussed.

2. Synthesis of metal–σ-borane complexes

2.1. Titanium complexes

Hartwig et al. [21], Muhoro and Hartwig [22] and Muhoro et al. [23] reported, for the first time, representative examples of the titanium–σ-borane complexes by the reaction of $[(\eta^5\text{-}C_5H_5)_2TiMe_2]$ with catecholborane or a substituted catecholborane (**1**–**7**). The reaction of complex **(1)** with $[(\eta^5\text{-}C_5H_5)_2Ti(PMe_3)_2]$ in toluene resulted in the formation of complex $[(\eta^5\text{-}C_5H_5)_2Ti(HBcat)(PMe_3)]$ **(8)**. Complexes **(9)** and **(10)** were prepared similarly by the reaction of complex **(2)** with $[(\eta^5\text{-}C_5H_5)_2Ti(PMe_3)_2]$ and complex **(7)** with $[(\eta^5\text{-}C_5H_5)_2Ti(PMe_3)_2]$ respectively. Reaction of complex **(2)** with phenylsilane in toluene yielded complex $[(\eta^5\text{-}C_5H_5)_2Ti(HBcat\text{-}4\text{-}t\text{-}Bu)(SiH_3Ph)]$ **(11)**.

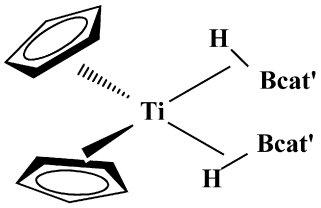

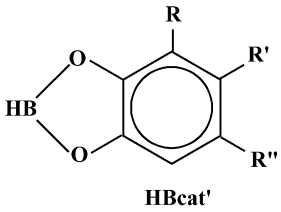

HBcat'

(1) R = H, R' = H, R" = H; **(2)** R = H, R' = H, R" = t-Bu
(3) R = t-Bu, R' = H, R" = t-Bu; **(4)** R = H, R' = H, R" = Me
(5) R = H, R' = H, R" = Cl; **(6)** R = H, R' = H, R" = SMe
(7) R = F, R' = H, R" = H

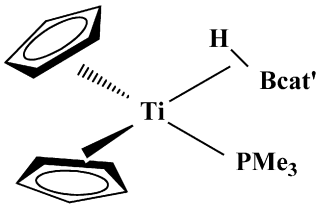

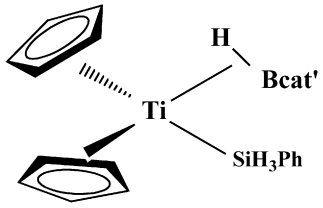

(8) R = H, R' = H, R" = H;
(9) R = H, R' = H, R" = t-Bu
(10) R = F, R' = H, R" = H

(11) R = H, R' = H, R" = t-Bu

2.2. Manganese and rhenium complexes

Manganese complexes $[(\eta^5\text{-}MeC_5H_4)Mn(CO)_2(HBcat)]$ **(12)** and $[(\eta^5\text{-}MeC_5H_4)Mn(CO)_2(HBpin)]$ **(13)** are prepared by photolysis of $[(\eta^5\text{-}MeC_5H_4)Mn(CO)_3]$ in THF in the presence of excess of the borane ligands HBcat and HBpin, respectively. Reaction of $K[(\eta^5\text{-}MeC_5H_4)Mn(CO)_2H]$ with ClBcat or ClBpin in pentane also produces complexes **(12)** and **(13)**. $BrBMe_2$ reacts with $K[(\eta^5\text{-}MeC_5H_4)Mn(CO)_2H]$ in pentane to give $[(\eta^5\text{-}MeC_5H_4)Mn(CO)_2(HBMe_2)]$ **(14)**. Similarly, reaction of $ClBCy_2$ with $K[(\eta^5\text{-}MeC_5H_4)Mn(CO)_2H]$ results in the formation of borane complex $[(\eta^5\text{-}MeC_5H_4)Mn(CO)_2(HBCy2)]$ **(15)** [24]. Rhenium borane complex $[(\eta^5\text{-}C_5Me_5)Re(CO)_2(HBpin)]$ is formed when $[(\eta^5\text{-}C_5Me_5)Re(CO)_2(Bpin)_2]$ **(16)** with methanol in benzene [24].

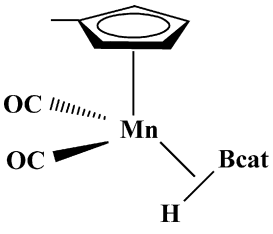

(12)

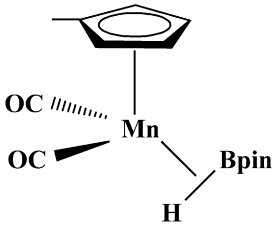

(13)

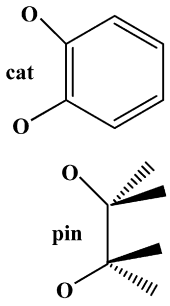

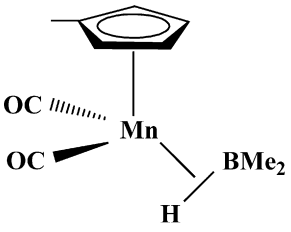

(14)

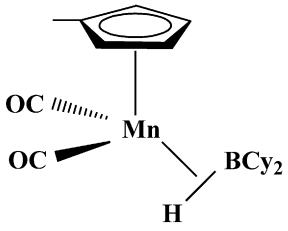

(15)

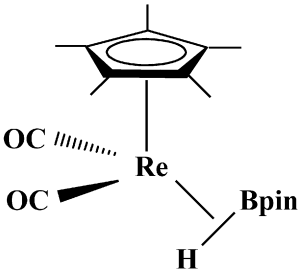

(16)

2.3. Ruthenium complexes

Reaction of $[RuH_2(H_2)_2(PCy_3)_2]$ with excess pinacolborane at room temperature yields the ruthenium borane complex $[RuH[(H_2Bpin](HBpin)(PCy_3)_2$ (**17**) [27]. The stoichiometric reaction of $[RuH_2(H_2)_2(PCy_3)_2]$ with HBpin in toluene results in the formation of $[RuH_2(HBpin)(H_2)(PCy_3)_2]$ **(18)**. Similarly, $[RuH_2(H_2)_2(PCy_3)_2]$ reacts with 1.1 equivalent of HBcat in pentane to give ruthenium borane complex $[RuH_2(HBcat)(H_2)(PCy_3)_2]$ **(19)** [28].

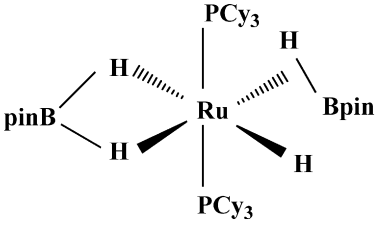

(17)

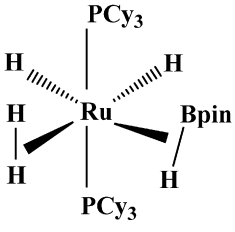

(18)

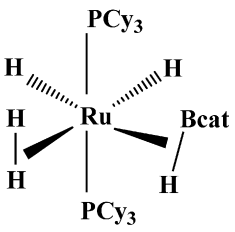

(19)

2.4. Nickel complexes

Reaction of two equivalent of substituted diphenylethane nickel hydride complexes $[(R_2PCH_2CH_2PR_2)NiH]$ (R = Cy, iPr, t-Bu) with a mixture of $LiHBEt_3$ and BEt_3 results in the formation of nickel(o) borane complexes $[(Cy_2PCH_2CH_2PCy_2)Ni(HBEt_2)]$ **(20)**, $[(iPr_2PCH_2CH_2PiPr_2)Ni(HBEt_2)]$ **(21)** and $[(tBu_2PCH_2CH_2PtBu_2)Ni(HBEt_2)]$ **(22)**. Complexes **(20)**, **(21)** and **(22)** are also prepared in low yield by the reaction of $[(R_2PCH_2CH_2PR_2)NiH]$ with $(HBEt_2)_2$ in THF [29].

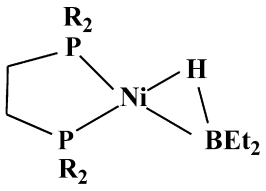

(20), R = Cy; (21), R = iPr; (22), R = t-Bu

3. Elongated metal–σ-borane complexes

A few metal–σ-borane complexes containing elongated B···H bond have been synthesized and characterized. Thermal or photochemical reaction of $[(\eta^5\text{-}C_5Me_5)Rh(H)_2(SiEt_3)_2]$ with HBpin results in the formation of $[(\eta^5\text{-}C_5Me_5)Rh(H)_2(SiEt_3)(Bpin)]$ **(23)** [30]. Hartwig et al. have reported that the photochemical reaction of HBpin in cyclohexane with $[(\eta^5\text{-}C_5Me_5)Rh(\eta^4\text{-}C_6Me_6)]$ yields hydride boryl complex $[(\eta^5\text{-}C_5Me_5)Rh(H)_2(Bpin)_2]$ **(24)**, which reacts in neat HBpin to give $[(\eta^5\text{-}C_5Me_5)Rh(H)(Bpin)_3]$ **(25)** [31]. Photochemical reactions of $[(\eta^5\text{-}C_5H_5)Rh(PR_3)(C_2H_4)]$ (R = Me, Ph) in hexane with HBpin give the hydride boryl complexes $[(\eta^5\text{-}C_5H_5)Rh(H)(Bpin)(PR_3)]$ (**26**, R = Me; **27**, R = Ph) having some residual B···H interaction [53]. Smith et al. have synthesized iridium complex $[(\eta^5\text{-}C_5Me_5)Ir(H)(Bpin)(PMe_3)]$ **(28)** by the reaction of $[(\eta^5\text{-}C_5Me_5)Ir(H)(Cy)(PR_3)]$ with HBpin in cyclohexane [35b]. Hydridoborate complexes are common [60,61] and have residual B···H interactions when the boron contains alkoxo groups.

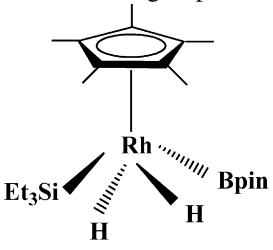

(23)

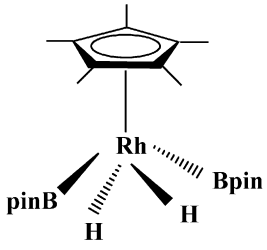

(24)

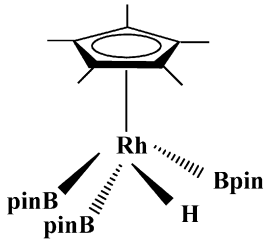

(25)

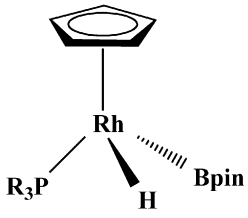

(26, R = Me; 27, R =Ph)

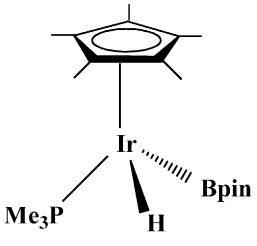

(28)

4. Reactivity of metal–σ-borane complexes

Ligand substitution reactions for Bcat ligand in borane complexes $[(\eta^5\text{-}C_5H_5)_2Ti(Hbcat\text{-}4\text{-}t\text{-}Bu)_2]$ and $[(\eta^5\text{-}MeC_5H_4)Mn(CO)_2(HBcat)]$ have been investigated by Muhoro et al. [23] and Schlecht and Hartwig [24]:

$[(\eta^5\text{-}C_5H_5)_2Ti(HBcat\text{-}4\text{-}t\text{-}Bu)_2] + PMe_3 \rightarrow [(\eta^5\text{-}C_5H_5)_2Ti(HBcat\text{-}4\text{-}t\text{-}Bu)(PMe_3)]$

$[(\eta^5\text{-}C_5H_5)_2Ti(HBcat\text{-}4\text{-}t\text{-}Bu)_2] + 2CO \rightarrow [(\eta^5\text{-}C_5H_5)_2Ti(CO)_2]$

$[(\eta^5\text{-}C_5H_5)_2Ti(HBcat\text{-}4\text{-}t\text{-}Bu)_2] + PhSiH_3 \rightarrow [(\eta^5\text{-}C_5H_5)_2Ti(HBcat\text{-}4\text{-}t\text{-}Bu)(PhSiH_3)]$

$[(\eta^5\text{-}C_5H_5)_2Ti(HBcat\text{-}4\text{-}t\text{-}Bu)_2] + PhC_2H_2Ph \rightarrow [(\eta^5\text{-}C_5H_5)_2Ti(HBcat\text{-}4\text{-}t\text{-}Bu)(PhC_2H_2Ph)]$

$[(\eta^5\text{-}MeC_5H_4)Mn(CO)_2(HBcat)] + HBpin \rightarrow [(\eta^5\text{-}MeC_5H_4)Mn(CO)_2(HBpin)]$

$[(\eta^5\text{-}MeC_5H_4)Mn(CO)_2(HBcat)] + HSiPh_2Me \rightarrow [(\eta^5\text{-}MeC_5H_4)Mn(CO)_2H(SiPh_2Me)]$

$[(\eta^5\text{-}MeC_5H_4)Mn(CO)_2(HBcat)] + PhC2H2Ph \rightarrow [(\eta^5\text{-}MeC_5H_4)Mn(CO)_2(PhC_2H_2Ph)]$

$[(\eta^5\text{-}MeC_5H_4)Mn(CO)_2(HBcat)] + CO \rightarrow [(\eta^5\text{-}MeC_5H_4)Mn(CO)_3]$

5. Spectroscopic studies

Infrared frequency, ^1H NMR and ^{11}B NMR spectral data of the σ-borane complexes are presented in Table 1. The IR spectra of the σ-borane complexes exhibit a medium intense band in region 1592–1773 cm^{-1}, which is described as a $\nu_{(H-B)}$. Decrease in $\nu_{(H-B)}$ on coordination of a borane ligand to transition metal and variation in $\nu_{(H-B)}$ frequencies depend on the extent of activation of the B–H bond upon coordination. The larger the value of $\nu_{(H-B)}$, the smaller the activation of B–H bond.

The ^{11}B NMR signals of the σ-borane complexes in the region 35–65 ppm are downfield of free borane ligands, but upfield of isolated metallocene boryl complexes. These observations reveal the partial metal-boron bond character. The trend in ^{11}B NMR signals in borane complexes **(1)**, **(2)**, **(7)** and **(8)**, **(9)**, **(10)** is attributed to differences in electron density at titanium and boron atoms in the two set of complexes. The ^1H NMR spectra of σ-borane complexes show a broad hydride signal approximately in the range −5 to −17 ppm due to interaction with the boron atom. These signals sharpen upon decoupling from boron.

6. X-ray crystal structural studies

The metal–σ-borane complexes, which have been structurally characterized, are listed in Table 2. In general, the M–B bond distances of the borane complexes are longer than those expected for single bond based on sum of covalent radii (Ti–B = 2.16 Å, Mn–B = 2.05 Å, Ru–B = 2.13 Å) while for elongated borane complexes, the Rh–B bond distances are shorter than the sum of covalent radii (Rh–B = 2.09 Å). The difference in bond distances and bond angles between the complexes $[\eta^5\text{-}C_5H_5)Ti(\eta^2\text{-}HBcat)_2]$ and $[\eta^5\text{-}C_5H_5)Ti(\eta^2\text{-}HBcat\text{-}4\text{-}F)(PMe_3)]$ may be due to differences in electron density at the titanium atom in the two complexes. Upon substituting HBcat for HBpin, the M–B bond distances in manganese

Table 1
Important IR frequencies (cm^{-1}) and ^1H NMR and ^{11}B NMR spectral data of transition metal–σ-borane complexes

Complex	υ(M-H-B) (cm^{-1})	^1H NMR δ (ppm)	^{11}B NMR δ (ppm)	Reference
σ-borane complexes				
$[\eta^5\text{-}C_5H_5)_2Ti(\eta^2\text{-}HBcat)_2]$	1611	−5.85	45.0	[23]
$[\eta^5\text{-}C_5H_5)_2Ti(\eta^2\text{-}HBcat\text{-}4\text{-}t\text{-}Bu)_2]$	1603	−5.67	46.0	[23]
$[\eta^5\text{-}C_5H_5)_2Ti(\eta^2\text{-}HBcat\text{-}3,5\text{-}t\text{-}Bu)_2]$	1621	−5.37	46.3	[23]
$[\eta^5\text{-}C_5H_5)_2Ti(\eta^2\text{-}HBcat\text{-}4\text{-}Me)_2]$	1611	−5.45	45.8	[23]
$[\eta^5\text{-}C_5H_5)_2Ti(\eta^2\text{-}HBcat\text{-}4\text{-}Cl)_2]$	1599	−5.80	45.8	[23]
$[\eta^5\text{-}C_5H_5)_2Ti(\eta^2\text{-}HBcat\text{-}4\text{-}SMe)_2]$	1599	−5.83	45.7	[23]
$[\eta^5\text{-}C_5H_5)_2Ti(\eta^2\text{-}HBcat\text{-}4\text{-}F)_2]$	1626	−5.80	45.7	[23]
$[\eta^5\text{-}C_5H_5)_2Ti(\eta^2\text{-}HBcat)(PMe_3)]$	1650	−9.80	64.2	[23]
$[\eta^5\text{-}C_5H_5)_2Ti(\eta^2\text{-}HBcat\text{-}4\text{-}t\text{-}Bu)(PMe_3)]$		−9.70	64.0	[23]
$[\eta^5\text{-}C_5H_5)_2Ti(\eta^2\text{-}HBcat\text{-}4\text{-}F)(PMe_3)]$		−9.40	64.9	[23]
$[\eta^5\text{-}C_5H_5)_2Ti(\eta^2\text{-}HBcat\text{-}4\text{-}t\text{-}Bu)(SiH_3Ph)]$	1773	−6.78	37.1	[23]
$[\eta^5\text{-}MeC_5H_4)Mn(CO)_2(\eta^2\text{-}HBcat)]$	1606	−14.46	46.0	[24]
$[\eta^5\text{-}MeC_5H_4)Mn(CO)_2(\eta^2\text{-}HBpin)]$	1603	−15.66	45.0	[24]
$[\eta^5\text{-}MeC_5H_4)Mn(CO)_2(\eta^2\text{-}HBMe_2)]$	1592	−17.06	101	[24]
$[\eta^5\text{-}MeC_5H_4)Mn(CO)_2(\eta^2\text{-}HBCy_2)]$	1597	−16.96	104	[24]
$[\eta^5\text{-}C_5Me_5)Re(CO)_2(\eta^2\text{-}HBpin)]$	1603	−11.06	46.0	[24]
$[RuH(H_2Bpin)(\eta^2\text{-}HBpin)(PCy_3)_2]$		−7.13	37.3	[27]
$[RuH_2(\eta^2\text{-}HBpin)(\eta^2\text{-}H_2)(PCy_3)_2]$		−8.83	35.1	[28]
$[RuH_2(\eta^2\text{-}HBcat)(\eta^2\text{-}H_2)(PCy_3)_2]$		−8.48	35.8	[28]
$[(Cy_2PCH_2CH_2PCy_2)Ni(\eta^2\text{-}HBEt_2)]$		−7.00	43.32	[29]
$[(iPr_2PCH_2CH_2PiPr_2)Ni(\eta^2\text{-}HBEt_2)]$		−6.96	45.38	[29]
$[(tBu_2PCH_2CH_2PtBu_2)Ni(\eta^2\text{-}HBEt_2)]$		−7.50	48.0	[29]
Elongated σ-borane complexes				
$[\eta^5\text{-}C_5Me_5)Rh(H)_2(Bpin)_2]$		−11.9	40.4	[31]
$[\eta^5\text{-}C_5Me_5)RhH(Bpin)_3]$		−11.3	39.9	[31]
$[\eta^5\text{-}C_5Me_5)RhH(Bpin)(PMe_3)]$		−14.04	45.4	[54]
$[\eta^5\text{-}C_5Me_5)RhH(Bpin)(PPh_3)]$		−13.04	44.8	[54]
$[\eta^5\text{-}C_5Me_5)IrH(Bpin)(PMe_3)]$		−17.64	33.0	[34b]

and ruthenium complexes are significantly shorter. The better π-acceptor character of HBcat compared to HBpin is responsible for a stronger M-B bond. As pointed out by Eisenstein et al. [11] the X-ray diffraction method does not properly locate a hydrogen center. The borane complexes contain extremely small H–M–B bond angles. The B–H bond distances are also longer than the sum of covalent radii (1.19 Å). More detailed description of M–H, B–H and H–M–B will be discussed in bonding section.

7. Theoretical studies

Theoretical calculations have been performed for σ-borane complexes of titanium [21,40,62,63], manganese [64], rhenium [65], ruthenium [28,63], nickel [66] and rhodium [67] as well as σ-borate complexes $[(\eta^5\text{-}C_5H_5)_2Nb\{H_2B(OH)_2\}]$ [68], $[(\eta^5\text{-}C_5H_5)_2Nb\{H_2B(C_8H_{14})\}]$ and $[\eta^5\text{-}C_5H_5)_2Nb\{H_2B(H)_2\}]$ [69].

The possible valence bond representations for M-HBR_2 moiety is presented in Chart 1. A main question concerns whether

Table 2
X-ray structural data for transition metal–σ-borane complexes

Complex	M–B (Å)	M–H (Å)	B–H (Å)	M–B–H (°)	B–M–H (°)	M–H–B (°)	Reference
σ-borane complexes							
$[\eta^5\text{-}C_5H_5)_2Ti(\eta^2\text{-}HBcat)_2]$	2.335(5)	1.74(4)	1.25(3)	47(2)	32(1)	101(2)	[21,23]
$[\eta^5\text{-}C_5H_5)_2Ti(\eta^2\text{-}HBcat\text{-}4\text{-}F)_2(PMe_3)]$	2.267(6)	1.61(5)	1.35(5)	44(2)	36(2)		[22,23]
$[\eta^5\text{-}MeC_5H_4)Mn(CO)_2(\eta^2\text{-}HBcat)]$	2.083(2)	1.57(2)	1.29(2)	48.6(7)	38.2(6)		[24]
$[\eta^5\text{-}MeC_5H_4)Mn(CO)_2(\eta^2\text{-}HBpin)]$	2.149(2)	1.53(2)	1.31(2)	44.7(9)	37.2(8)		[24]
$[\eta^5\text{-}MeC_5H_4)Mn(CO)_2(\eta^2\text{-}HBCy_2)]$	2.187(3)	1.49(2)	1.24(2)	41.1(9)	33.2(7)		[24]
$[RuH(H_2Bpin)(\eta^2\text{-}HBpin)(PCy_3)_2]$	2.157(5)	1.58(3)	1.35(3)		38.6(11)	94.4(20)	[27]
$[RuH_2(\eta^2\text{-}HBpin)(\eta^2\text{-}H_2)(PCy_3)_2]$	2.173(2)	1.67(2)	1.30(2)	50.1(8)		93.28(6)	[28]
$[RuH_2(\eta^2\text{-}HBcat)(\eta^2\text{-}H_2)(PCy_3)_2]$	2.124(2)	1.71(2)	1.24(2)	53.7(8)		90.6(7)	[28]
$[(Cy_2PCH_2CH_2PCy_2)Ni(\eta^2\text{-}HBEt_2)]$	2.172(6)	1.47(5)	1.23(5)	40.69	32.77	106.54	[29]
Elongated σ-borane complexes							
$[\eta^5\text{-}C_5Me_5)Rh(H)_2(Bpin)_2]$	2.055(7)	1.47(6)	1.65(4)		53.1(17)		[31]
	2.081(6)	1.59(6)	1.70(6)		53(2)		
$[\eta^5\text{-}C_5Me_5)RhH(Bpin)_3]$	2.059(3)	1.47(3)	1.69(3)		54.3(10)		[31]
$[\eta^5\text{-}C_5Me_5)RhH(Bpin)(PPh_3)]$	2.0196(15)	1.50(2)	2.09(2)		71.0(8)		[54]

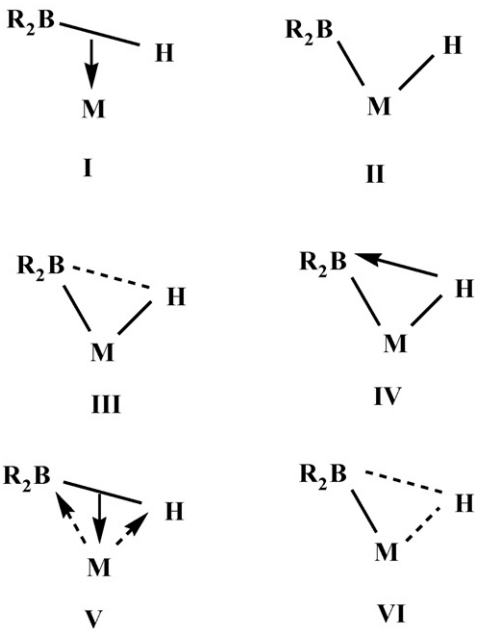

Chart 1. The possible valence bond representations for M-HBR_2.

the bonding tends more towards the σ-borane complex **I** or to the classical oxidative addition product hydride boryl complex **II**. Structures **III** and **IV** are consistent with structure **II** with some residual B–H interaction. Structure **V** favors appreciable retention of B–H bond as in structure **I** with substantial donation of metal electron density to the borane by M → B back-bonding. Structure **VI** represents the hydride as bridging between the M and B centers with a three center-two electron bond. The three center-two electron bond in M–H–B bridge may be regarded as a "protonated π-bond". This description is in accord with the 3c–2e bond study of Lammertsma and Ohwada [70]. Many factors can affect the relative stabilities of structures I and II, such as behavior of the ancillary ligands, substitutions on the boron atom and the replacement of one metal center by other. A number of elongated dihydrogen complexes with H···H distances between 1 and 1.5 Å (representing structures **III** and **IV**) have been reported [11,71–73].

7.1. Theoretical methods

Theoretical work concerning the nature of the M-(η^2-HBR_2) bond used either standard *ab initio* calculations or gradient corrected DFT methods. The details of the methods can be found in the original papers. The methods for energy decomposition analysis shall be discussed briefly.

The geometry optimizations and bond energy decomposition analysis were performed at the nonlocal DFT level of theory using the exchange functional of Becke [74] and the correlation functional of Perdew [75] (BP86). Scalar relativistic effects have been considered using the ZORA formalism [76]. Uncontracted Slater-type orbitals (STOs) were used as basis functions for the SCF calculations [77]. Triple-ζ basis sets augmented by two sets of polarization function have been used for all the elements. The calculations were carried out using the program package ADF-2004 and ADF-2006 [78]. The bonding interactions between the fragments [M] and [HBR_2] have been analyzed using the energy decomposition scheme of ADF which is based on the methods of Morokuma [79] and Ziegler and Rauk [80]. The bond dissociation energy ΔE between two fragments [M] and [HBR_2] is partitioned into several contributions that can be identified as physically meaningful entities. First, ΔE is separated into two major components ΔE_{prep} and ΔE_{int}:

$$\Delta E = \Delta E_{prep} + \Delta E_{int} \quad (1)$$

Here, ΔE_{prep} is the energy that is necessary to promote both fragments from their equilibrium geometry and electronic ground state to the geometry and electronic state that they have in the combined molecule.

$$\Delta E_{prep} = E_{total}\ \text{(distorted fragments)} - E_{total}\ \text{(fragments in the equilibrium structure)} \quad (2)$$

ΔE_{int} is the interaction energy between the two fragments in the molecule. The interaction energy, ΔE_{int}, can be divided into three main components:

$$\Delta E_{int} = \Delta E_{elstat} + \Delta E_{Pauli} + \Delta E_{orb} \quad (3)$$

ΔE_{elstat} is the electrostatic interaction of the nuclear charge and unmodified charge density on one fragment with the nuclear charge and unmodified charge density of the other fragments. ΔE_{elstat} stabilizes the bond between two fragments. The second term in Eq. (3) ΔE_{Pauli} which is called exchange repulsion or Pauli repulsion, gives the repulsive interactions between the fragments that are due to the fact that two electrons with the same spin cannot occupy the same region in space. The term comprises the four-electron destabilizing interactions between occupied orbitals. ΔE_{Pauli} is calculated by enforcing the Kohn–Sham determinant of the molecule, which results from superimposing both fragments, to obey the Pauli principle through antisymmetrization and renormalization. The stabilizing orbital interaction term ΔE_{orb} is calculated in the final step of the energy analysis when the Kohn–Sham orbitals relax to their optimal form. The latter term can be further partitioned into contributions by the orbitals that belong to different irreducible representations of the point group of the system. The covalent and electrostatic character of the bond is given by the ratio $\Delta E_{elstat}/\Delta E_{orb}$.

7.2. Bonding in titanium–σ-borane complexes

Eisenstein and co-workers optimized the geometry of a model titanium–σ-borane complex [(η^5-C_5H_5)Ti($HB(OH)_2)_2$] using core potential *ab initio* second order Møller–Plesset perturbation theory (MP2) [21]. The calculation confirms that the boron atom is not tetrahedral. The geometrical parameters have not been reported. Lam and Lin [62] have investigated the bonding analysis of model titanium–σ-borane complexes [(η^5-$C_5H_5)_2$Ti($HB(OH)_2)_2$] and [(η^5-$C_5H_5)_2$Ti($HB(OH)_2$)(PH_3)] using DFT/B3PW91 level of theory. In the model complexes the steric bulk of the substituted phosphine ligand and HBcat ligand

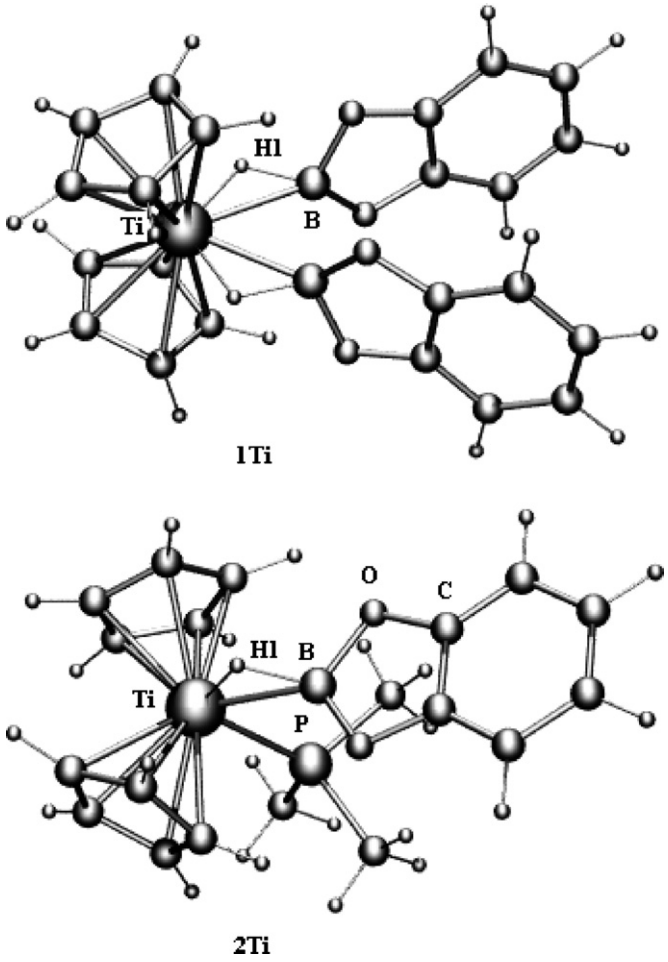

Fig. 1. Optimized geometries of the titanium–σ-complexes $[(\eta^5\text{-}C_5H_5)_2Ti(\eta^2\text{-}HBcat)_2]$ **1Ti** and $[(\eta^5\text{-}C_5H_5)_2Ti(\eta^2\text{-}HBcat)(PMe_3)]$ **2Ti**.

were modeled as PH_3 and $HB(OH)_2$, respectively. Geometries of the real titanium–σ-borane complexes $[(\eta^5\text{-}C_5H_5)_2Ti(HBcat)_2]$ **1Ti** and $[(\eta^5\text{-}C_5H_5)_2Ti(HBcat)(PMe_3)]$ **2Ti** have been calculated at DFT/BP86 level [63]. The optimized structures of **1Ti** and **2Ti** (Fig. 1, Table 3) closely resemble the experimental results (Table 2). There is little difference in geometries between the real complexes **1Ti** and **2Ti** and model complexes **3Ti** and **4Ti** (Table 3). The results reveal that both the small and large ligands give reasonable agreement with experimental results. The Ti–B bond distances 2.364 Å in **1Ti** and 2.294 Å in **2Ti** are too long to be true metal boryl bond and the B–Ti–B angle 53.4° in **1Ti** is too small for the compound to be considered a Ti(IV) complex. The Ti–H bond distances 1.798 Å in **1Ti** and 1.791 Å in **2Ti** are typical for bridging hydride complex. The geometrical data are consistent with complexes **1Ti** and **2Ti** being Ti(II) complexes in which both hydrogen and boron have bonding interaction with titanium atom while preserving B–H bond character. The Ti–B bond distance of 2.294 Å in **2Ti** is significantly shorter than 2.365 Å in **1Ti**. The better π-accepter character of phosphine ligand compared to HBcat is responsible for a stronger Ti–B bond in **2Ti** complex. Lin and co-workers have investigated the structure and stability of titanocene–σ-borane complexes $[(\eta^5\text{-}C_5H_5)_2Ti\{HB(OCH)_2)_2]$, $[(\eta^5\text{-}C_5H_5)_2Ti(HB(OCH)_2)L]$ (L=HC≡CH, $H_2C{=}CH_2$, SiH_4, CH_4 and H_2) using B3LYP [40]. The alkyne and alkene interact with boron of the borane ligand to form five membered-ring structures, while the silane, alkane and dihydrogen interact with boron to form hydroborato structures.

Table 3
Calculated geometrical parameters[a] for titanium–σ-borane complexes $[\eta^5\text{-}C_5H_5)_2Ti(\eta^2\text{-}HBcat)_2]$ **1Ti**, $[\eta^5\text{-}C_5H_5)_2Ti(\eta^2\text{-}HBcat)(PMe_3)]$ **2Ti** at BP86/TZ2P and model complexes $[\eta^5\text{-}C_5H_5)_2Ti\{\eta^2\text{-}HB(OH)_2\}_2]$ **3Ti**, $[\eta^5\text{-}C_5H_5)_2Ti(\eta^2\text{-}HB(OH)_2)(PH_3)]$ **4Ti** at B3PW91[b]

	1Ti	2Ti	3Ti	4Ti
Bond distances				
Ti–B	2.364	2.294	2.358(2.333)[c]	2.356
Ti–H1	1.798	1.791	1.724(1.746)	1.750
Ti–P		2.550		2.511
B–H1	1.317	1.336	1.344(1.322)	1.325
B–B	2.124		2.194(2.110)	
Bond angles				
Ti–H1–B	97.5	93.2		
Ti–B–H1	48.9	51.2		
B–Ti–H1	33.6	35.6		
B–Ti–B	53.4		55.5(54.4)	
P–Ti–B		74.9		73.5

[a] Distances are in Å and angles in degree.
[b] LANL2DZ basis set for Ti and P with Hay and Wadt effective core potentials and 6-31G basis set for H, B, C and O atoms [62].
[c] Values in parentheses are for the model complex $[\eta^5\text{-}C_5H_5)_2Ti\{\eta^2\text{-}HB(OCH)_2\}_2]$ at B3LYP using SDDall basis set for Ti and 6-31G basis set for H, B, C and O atoms [40].

7.3. Bonding in manganese–σ-borane complexes

Fig. 2 shows the optimized geometries of the manganese–σ-borane complexes $[(\eta^5\text{-}MeC_5H_4)Mn(CO)_2(HBcat)]$ **1Mn**, $[(\eta^5\text{-}MeC_5H_4)Mn(CO)_2(HBpin)]$ **2Mn**, $[(\eta^5\text{-}MeC_5H_4)Mn(CO)_2(HBMe_2)]$ **3Mn**. The optimized bond lengths and angles at B3LYP and BP86 are presented in Table 4 [64]. The optimized structures of **1Mn**, **2Mn** and **3Mn** closely resemble that found by X-ray diffraction for **(12)**, **(13)** and **(15)** [24]. The Mn–B bond distances 2.106 Å in **1Mn**, 2.152 Å in **2Mn** and 2.168 Å in **3Mn** are longer than that expected for single bond based on covalent radius predictions (2.05 Å) [81]. Using the relationship between covalent bond order and bond distance suggested by Pauling we find the calculated Mn–B distances correspond to a covalent bond order of 0.80 in 1, 0.67 in 2, 0.63 in 3 [82]. The B–H bond distances 1.306 Å in **1Mn**, 1.312 Å in **2Mn** and 1.311 Å in **3Mn** are also longer than sum of covalent radii (1.19 Å) and those obtained by theoretical study for the free borane ligands (1.184 Å in HBcat, 1.190 Å in HBpin and 1.204 Å in $HBMe_2$). The optimized B–H bond distances in the σ-borane complexes correspond to a covalent bond order of about 2/3. The B–Mn–H1 bond angles are very small and are consistent with B–H bonding. These results are consistent with **1Mn**, **2Mn** and **3Mn** being Mn(I) complexes in which both hydrogen and boron of the $[HBR_2]$ ligands have a bonding interaction with the manganese preserving B–H bond character.

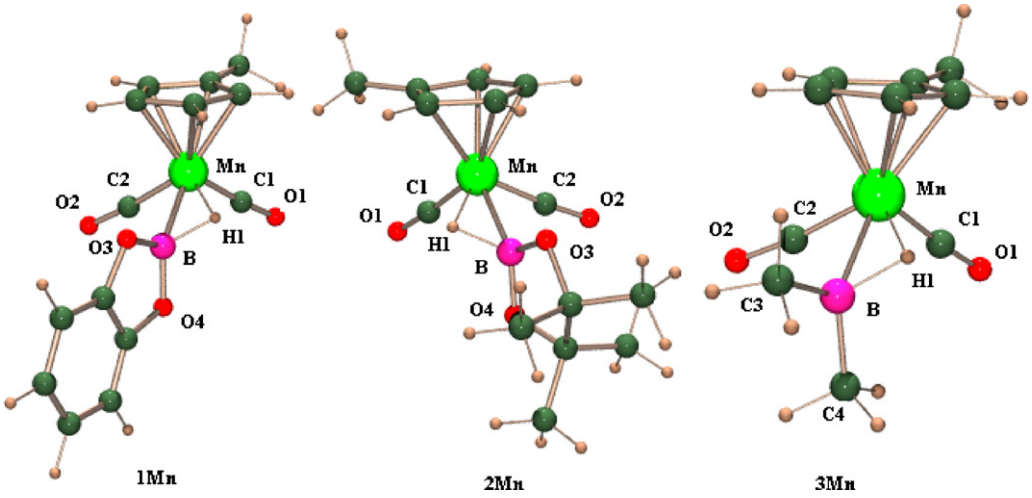

Fig. 2. Optimized geometries of the manganese–σ-complexes $[(\eta^5\text{-}MeC_5H_4)Mn(CO)_2(\eta^2\text{-}HBR_2)]$ (**1Mn**, R_2 = Bcat; **2Mn**, R_2 = Bpin; **3Mn**, R2 = Me_2).

Table 5 gives the Wiberg bond indices [83] (WBI), which provide bond orders, and the natural bond orbital (NBO) analysis. The Wiberg bond indices values of the Mn–B bonds of the complexes **1Mn**–**3Mn** are small ∼0.45. Upon Coordination of the borane ligand, the B–H bond orders are calculated to be reduced by ∼1/3. The net electron transfer from the $[(\eta^5\text{-}MeC_5H_4)Mn(CO)_2]$ fragment to borane ligands HBcat (0.20 electron), HBpin (0.17 electron) and $HBMe_2$ (0.24 electron). The HBcat is a better π-acceptor compared to HBpin.

A more definitive picture of Mn–B, Mn–H and B–H bonding is obtained through NBO analysis of the delocalized Kohn–Sham orbitals. The characteristics of the Mn–B and M–H–B bonding orbitals are listed in Table 5. The occupancies of these orbitals are relatively low. The Mn–B bonding orbitals are polarized towards Mn, while the B–H bonding orbitals are polarized towards H. The coordination of a σ-borane ligand causes a rehybridization of the boron center. The hybrid orbital of boron along the B–H bond in the free ligand is $sp^{1.23}$ (HBcat), $sp^{1.50}$ (HBpin), $sp^{2.10}$ ($HBMe_2$) and in the borane complexes is $sp^{3.67}$ (1), $sp^{3.89}$ (2) and $sp^{4.16}$ (3). These results reveal that less 2s character and more 2p character goes to the B–H bond upon coordination of borane to manganese atom.

Table 6 shows the results of the energy decomposition analysis of the interaction energy ΔE_{int} of the combination

Table 4
Selected optimized geometrical parameters for manganese–σ-borane complexes $[(\eta^5\text{-}MeC_5H_4)Mn(CO)_2(\eta^2\text{-}HBR_2)]$ (**1Mn**, R_2 = cat; **2Mn**, R_2 = pin; **3Mn**, R = Me)[a], $[(\eta^5\text{-}MeC_5H_4)Mn(CO)_2]$, HBcat, HBpin, $HBMe_2$ (Calculations were done at both B3LYP/6-31(d) and BP86/TZ2P)

	1Mn	2Mn	3Mn	[(Cp′)Mn(CO)2]	HBcat	HBpin	HBMe2
Bond distances							
Mn–B	2.106(2.095)	2.152(2.141)	2.168(2.173)				
Mn–H1	1.602(1.604)	1.597(1.590)	1.620(1.609)				
Mn–C1	1.790(1.775)	1.773(1.767)	1.786(1.770)	1.787(1.776)			
Mn–C2	1.779(1.772)	1.786(1.775)	1.774(1.769)	1.784(1.775)			
B–H1	1.306(1.355)	1.312(1.367)	1.311(1.355)		1.184(1.186)	1.190(1.194)	1.204(1.208)
B–O3	1.403(1.413)	1.381(1.391)			1.384(1.389)	1.367(1.373)	
B–O4	1.405(1.418)	1.377(1.387)			1.384(1.389)	1.367(1.373)	
C1–O1	1.158(1.164)	1.163(1.169)	1.159(1.170)	1.161(1.169)			
C2–O2	1.161(1.165)	1.159(1.166)	1.164(1.167)	1.162(1.169)			
B–C3		1.587(1.587)					1.569(1.567)
B–C4		1.586(1.583)					1.569(1.567)
Bond angles							
Mn–H1–B	92.2(89.8)	94.9(92.5)	94.9(93.9)				
Mn–B–H1	49.5(50.0)	47.7(47.9)	48.1(47.6)				
B–Mn–H1	38.3(40.2)	37.4(39.6)	37.1(38.5)				
C1–Mn–C2	93.0(90.5)	91.5(89.7)	98.2(91.6)	96.4(93.9)			
O3–B–O4	110.1(109.6)	112.6(112.3)			111.9(112.1)	114.0(114.3)	
Mn–B–O3	126.9(127.4)	119.9 (120.4)		116.7(1)			
Mn–B–O4	121.3(121.9)	125.7(126.3)					
C3–B–C4			117.2(117.5)				124.3(122.2)
Mn–B-C3			119.0(118.8)				
Mn–B–C4			122.6(123.0)				

Values in the parentheses are obtained at BP86/TZ2P. Distances are in Å and angles in degrees.

Table 5
Wiberg bond indices, and results of the NBO analysis in [(η^5-MeC_5H_4)Mn(CO)$_2$(η^2-HBR$_2$)] complexes and in free ligands (B3LYP/6-31G(d))

	1Mn	2Mn	3Mn	HBcat	HBpin	HBMe$_2$
Wiberg bond indices						
Mn–B	0.46	0.43	0.45			
Mn–H1	0.25	0.28	0.25			
Mn–C1	1.08	1.05	1.10			
Mn–C2	1.01	1.09	1.10			
B–H	0.63	0.62	0.66	0.97	0.96	0.97
C1–O1	2.02	1.97	2.01			
C2–O2	1.99	2.01	1.96			
NBO analysis						
Mn–B Bond						
Occupancy	1.54	1.33	1.46			
Mn						
%	74.2	65.3	75.4			
%s	7.9	21.8	9.3			
%p	0.1	0.4	0.2			
%d	91.9	77.8	90.5			
B						
%s	29.5	27.6	15.4			
%p	78.4	72.3	84.3			
%d	0.1	0.1	0.2			
B–H bond						
Occupancy	1.66	1.65	1.66	1.98	1.98	1.98
B						
%	39.9	39.4	38.0	45.67	45.3	45.4
%s	21.4	20.4	19.3	44.7	39.9	32.3
%p	78.4	79.3	80.5	55.2	60.0	67.6
%d	0.2	0.3	0.2	0.1	0.1	0.1
H						
%s	100.0	100.0	100.0	100.0	100.0	100.0
Mn–H–B bond						
Occupancy	1.85	1.85	1.85			
Mn (%)	10.0	9.8	9.3			
H (%)	49.7	49.9	51.6			
B (%)	33.0	32.7	31.6			
NBO charges						
Mn	0.79	0.80	0.85			
B	0.72	0.74	0.38	0.92	0.92	0.69
H	−0.04	−0.05	−0.05	−0.08	−0.09	−0.09
R$_2$	−0.88	−0.86	−0.57	−0.84	−0.83	−0.60

Table 6
Energy decomposition analysis of [(η^5-MeC_5H_4)Mn(CO)$_2$(η^2-HBcat)] **1Mn**, [(η^5-MeC_5H_4)Mn(CO)$_2$(η^2-HBpin)] **2Mn** and [(η^5-MeC_5H_4)Mn(CO)$_2$(η^2-HBMe$_2$)] **3Mn** at BP86/TZ2P[a]

	1Mn	2Mn	3Mn
ΔE_{int}	−46.5	−44.4	−47.6
ΔE_{Pauli}	117.1	108.8	109.0
ΔE_{elstat}	−87.5	−84.6	−82.8
ΔE_{orb}[b]	−76.1 (46.5%)	−68.6 (44.8%)	−73.8 (47.1%)
ΔE_{prep}	16.1	15.1	13.3
$\Delta E(-D_e)$	−30.4	−29.3	−34.3

[a] Energy contributions in kcal/mol.
[b] The values in parentheses are the percentage contribution to the total attractive interactions reflecting the covalent character of the bond.

Table 7
Selected optimized geometrical parameters [BP86/TZ2P] for rhenium–σ-borane complexes [(η^5-MeC_5H_4)Re(CO)$_2$(η^2-HBcat)] **1Re**, [(η^5-MeC_5H_4)Re(CO)$_2$(η^2-HBpin)] **2Re** and [(η^5-MeC_5H_4)Re(CO)$_2$(η^2-HBMe$_2$)] **3Re** and [(η^5-MeC_5H_4)Re(CO)$_2$]

	1Re	2Re	3Re	[(η^5-MeC_5H_4)Re(CO)$_2$]
Bond distances				
Re–B	2.212	2.234	2.284	
Re–H1	1.730	1.703	1.725	
Re–C1	1.920	1.913	1.910	1.914
Re–C2	1.914	1.916	1.901	1.912
B–H1	1.445	1.479	1.422	
B–O3	1.417	1.393	1.589	
B–O4	1.410	1.387	1.589	
C1–O1	1.168	1.168	1.167	1.171
C2–O2	1.166	1.168	1.172	1.171
Bond angles				
Re–H1–B	87.8	88.8	92.5	
Re–B–H1	51.4	49.7	49.0	
B–Re–H1	40.8	41.5	38.5	
C1–Re–C2	89.4	86.6	88.7	92.2
O3–B–O4	112.0	109.6		
Re–B–O3	127.4	128.2		
Re–B–O4	120.2	121.4		
C3–B–C4			117.6	
Re–B–C3			124.2	
Re–B–C4			117.8	

Distances are in Å and angles in degrees.

of [(η^5-MeC_5H_4)Mn(CO)$_2$] and [HBR$_2$] into the three terms ΔE_{Pauli}, ΔE_{elstat}, and ΔE_{orb}. The bonding energies of compound **1Mn** (−30.44 kcal/mol), **2Mn** (−29.34 kcal/mol) and **3Mn** (−34.34 kcal/mol) are almost twice the mean value of metal-(η^2-H$_2$) bonding energies and larger than the experimental dissociation enthalpy for η^2-HBcat was found 25 ± 3 kcal/mol in [(η^5-MeC_5H_4)Mn(CO)$_2$(η^2-HBcat)] [24]. We note that, for Mn-η^2-H-BR$_2$ bonds in the complexes **1Mn**–**3Mn**, the contribution of electrostatic attractions ΔE_{elstat} are greater than the orbital interactions, ΔE_{orb}. The repulsive terms ΔE_{Pauli} were largest in each case. Table 6 shows that the trends of ΔE_{Pauli} and ΔE_{orb} from complexes **1Mn** to **3Mn** are roughly the same, while the ΔE_{elstat} values decrease for **1Mn** to **3Mn**. The [(η^5-MeC_5H_4)Mn(CO)$_2$]–[η^2-H-BR$_2$] bonding in manganese borane complexes is more than half electrostatic.

In order to visualize the Mn–B, B–H and Mn–B–H bonding, envelope plots of some relevant orbitals of [(η^5-MeC_5H_4)Mn(CO)$_2$(HBMe$_2$)] are shown in Fig. 3. Molecular orbital, Fig. 3A, is a well-formed Mn–H–B bond while molecular orbital, Fig. 3B, is a well-formed Mn–B bond. The Fig. 3C gives a pictorial description of the vacant π^* orbital.

7.4. Bonding in rhenium–σ-borane complexes

Fig. 4 shows the theoretically calculated geometries of the rhenium–σ-borane complexes [(η^5-MeC_5H_4)Re(CO)$_2$(η^2-HBcat)] **1Re**, [(η^5-MeC_5H_4)Re(CO)$_2$(η^2-HBpin)] **2Re**, [(η^5-MeC_5H_4)Re(CO)$_2$(η^2-HBMe$_2$)] **3Re**. The optimized bond lengths and angles are presented in Table 7 [65]. There are no X-ray structural data for rhenium complexes **1Re**-**3Re** known.

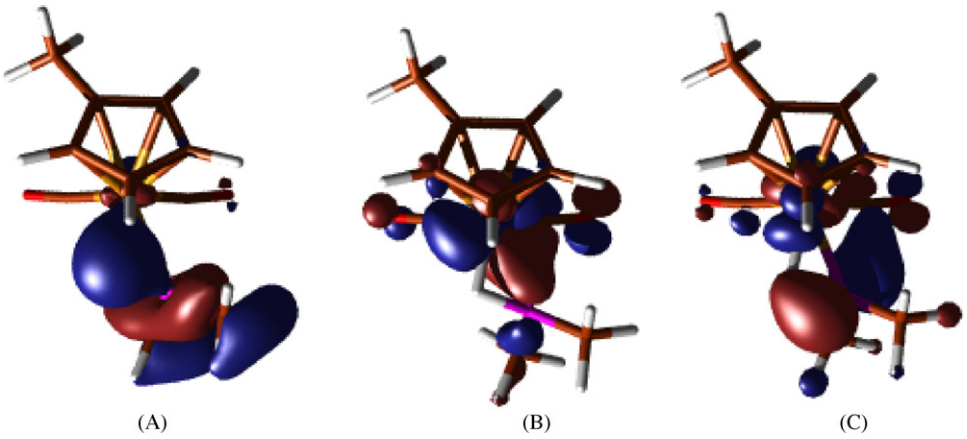

Fig. 3. Plot of some relevant molecular orbitals of $[\eta^5\text{-}MeC_5H_4)Mn(CO)_2(\eta^2\text{-}HBMe_2)]$.

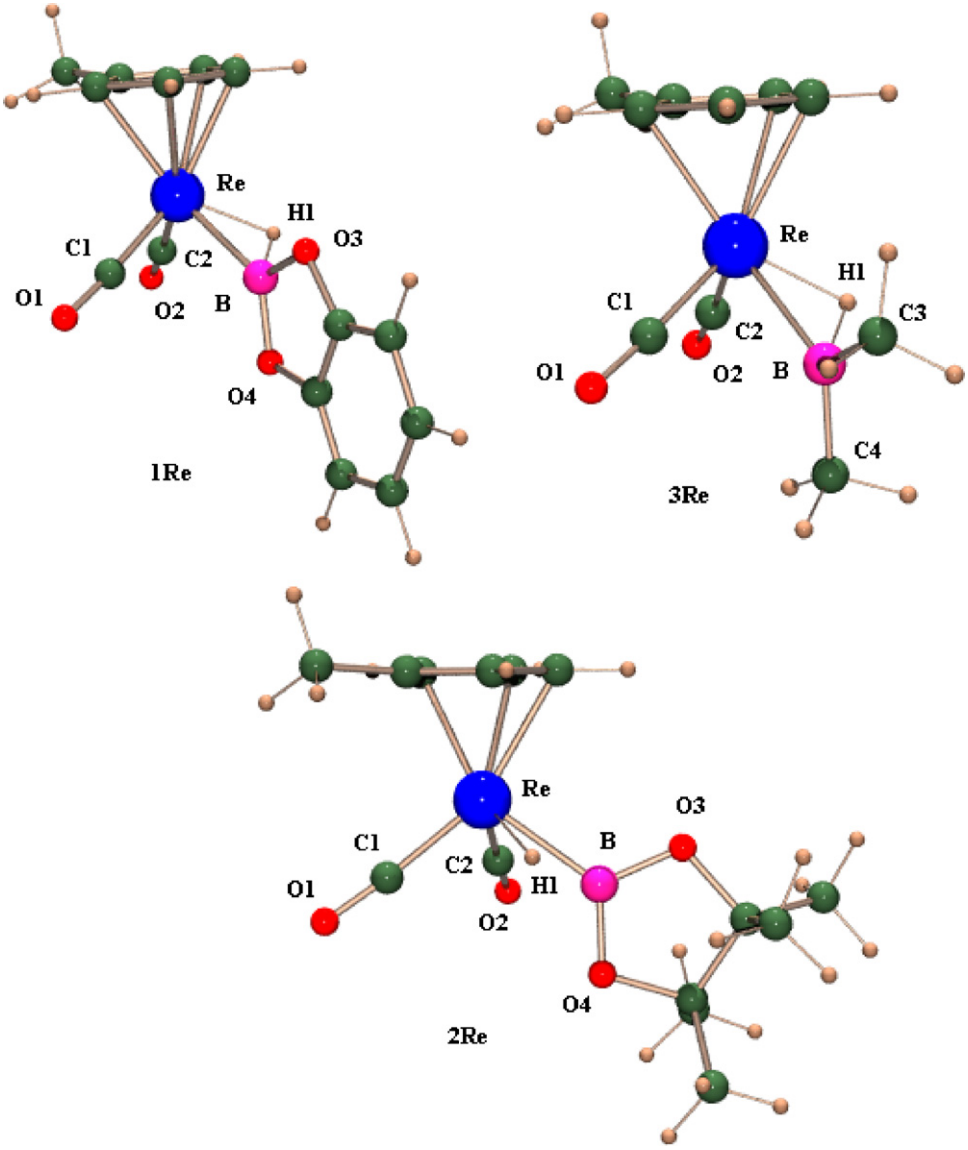

Fig. 4. Optimized geometries of $[(\eta^5\text{-}MeC_5H_4)Re(CO)_2(\eta^2\text{-}HBR_2)]$ (**1Re**, R_2 = Bcat; **2Re**, R_2 = Bpin; **3Re**, R2 = Me_2).

Table 8
Energy decomposition analysis of [(MeC_5H_4)Re(CO)$_2$(η^2-HBcat)] **1Re**, [(MeC_5H_4)Re(CO)$_2$(η^2-HBpin)] **2Re** and [(MeC_5H_4)Re(CO)$_2$(η^2-HBMe_2)] **3Re** at BP86/TZ2P[a]

	1Re	2Re	3Re
ΔE_{int}	−70.5	−73.6	−68.6
$\Delta E_{Pauling}$	170.5	176.8	156.7
ΔE_{elstat}	−135.0	−145.6	−126.7
ΔE_{orb}[b]	−106.0 (44.0%)	−104.8 (41.8%)	−98.6 (43.8%)
ΔE_{prep}	30.0	33.9	25.3
$\Delta E(-D_e)$	−40.5	−39.7	−43.3

[a] Energy contributions in kcal/mol.
[b] The values in parentheses are the percentage contribution to the total attractive interactions reflecting the covalent character of the bond.

We report here for the first time structures of these complexes. The Re–B bond distances 2.212 Å in **1Re**, 2.234 Å in **2Re** and 2.284 Å in **3Re** are longer than that expected for a single bond based on covalent radius predictions (2.10 Å) [81]. The B–H bond distances 1.445 Å in **1**, 1.479 Å in **2** and 1.422 Å in **3** are also longer than those calculated for corresponding manganese borane complexes **1Mn–3Mn**. The optimized B–H bond distances in rhenium–σ-borane complexes **1Re–3Re** correspond to a covalent bond order of about 1/2. The Re–H bond distances 1.730 Å in **1Re**, 1.703 Å in **2Re** and 1.725 Å in **3Re** are also longer than that expected for single bond based on covalent radius predictions (2.10 Å) [81]. The B–Re–H1 bond angles in the complexes [(η^5-MeC_5H_4)Re(CO)$_2$(η^2-HBR_2)]: 40.8° in **1Re**, 41.5° in **2Re** and 38.5° in **3Re** are small and are consistent with B–H bonding. These results are consistent with [(η^5-MeC_5H_4)Re(CO)$_2$(HBR_2)] being Re(I) complexes in which both hydrogen and boron of the [HBR_2] ligands have a bonding interaction with the rhenium preserving B–H bond character.

The theoretically predicted bond dissociation energies (Table 8) of the borane ligands are −40.5 kcal/mol for [(η^5-MeC_5H_4)Re(CO)$_2$(HBcat)], −39.7 kcal/mol for [(η^5-MeC_5H_4)Re(CO)$_2$(HBpin)]and −43.3 kcal/mol for [(η^5-MeC_5H_4)Re(CO)$_2$(HBMe_2)]. The breakdown of the rhenium–borane interaction energies into the different energy terms shows that the contribution of electrostatic attractions ΔE_{elstat} are greater than the orbital interactions, ΔE_{orb}. The repulsive terms ΔE_{Pauli} were largest in each case. Table 8 shows that the trends of ΔE_{Pauli} and ΔE_{elstat} from complexes **1Re** to **3Re** are roughly same, while the ΔE_{orb} values decrease for **1Re–3Re**. All three complexes exhibit about 42–44% covalent bonding of the borane ligand to the metal fragment.

7.5. Bonding in ruthenium–σ-borane complexes

Sabo-Etienne and co-workers investigated the structures of four isomers of each of the model ruthenium–σ-borane complexes [RuH_2(η^2-HBpin)(η^2-H_2)(PMe_3)$_2$] (**1RuBpin**–**4RuBpin**) and [RuH_2(η^2-HBcat)(η^2-H_2)(PMe_3)$_2$] (**1RuBcat**–**4RuBcat**) and two isomers of the complex [RuH{(μ-H)$_2$Bpin}(η^2-HBpin)(PMe_3)$_2$] (**5RuBpin**, **6RuBpin**) at DFT/B3LYP level. σ-H_2 rotation and σ-borane versus dihydridoborate ligation are intimately correlated [28]. The isomers of [RuH_2(η^2-HBpin)(η^2-H_2)(PMe_3)$_2$] are almost similar to the isomers of [RuH_2(η^2-HBcat)(η^2-H_2)(PMe_3)$_2$] (Fig. 5). The isomers **1RuBcat** and **2RuBcat** are degenerate, their energy difference is 4.6 kcal/mol. Similarly isomers **3RuBcat** and **4RuBcat** are degenerate with energy difference 1.0 kcal/mol. The isomers **1RuBpin** and **1RuBcat** correspond with the experimental structures [RuH_2(η^2-HBR)(η^2-H_2)(PCy_3)$_2$] (R = pin, cat) [28]. The optimized geometry of **5RuBpin** closely resembles the experimental geometry of [RuH{(μ-H)$_2$Bpin}(η^2-HBpin)(PCy_3)$_2$] [27]. The bis(dihydridoborate) isomer **6RuBpin** is at significant higher energy than 5RuBpin (energy difference is 16.0 kcal/mol). The geometries of ruthenium–σ-borane complexes **1RuBpin** and **1RuBcat** have been optimized using DFT/BP86 level of theory [63]. The optimized geometries are almost similar to the experimental values for ruthenium–σ-borane complexes [RuH_2(η^2-HBpin)(η^2-H_2)(PCy_3)$_2$] and [RuH_2(η^2-HBcat)(η^2-H_2)(PCy_3)$_2$] and to the optimized data obtained by Sabo-Etienne co-workers [28] (Table 9). The optimized structures of **1RuBpin** and **5RuBpin** are presented in Fig. 6.

7.6. Bonding in nickel, palladium and platinum–σ-borane complexes

Fig. 7 shows the optimized geometries of the borane complexes 1NiEt, 1PdEt, 1PtEt, 2NiMe, 2PdMe and 2PtMe. The optimized bond lengths and angles at BP86 are presented in Table 10 and Table 11 [66]. Theoretical studies for the free borane ligands have been obtained at the same level

Table 9
Selected optimized geometrical parameters for ruthenium–σ-borane complexes

Complex	M–B (Å)	M–H (Å)	B–H1 (Å)	M–B–H1 (°)	B–M–H1 (°)	M–H1–B (°)
1RuBpin	2.162(2.147)[a]	1.764(1.763)	1.362(1.371)	56.4(54.9)	37.1(40.6)	86.5(84.5)
2RuBpin	2.207	1.775	1.372	53.5	38.4	88.1
3RuBpin	2.276	1.750	1.320	50.0	35.4	94.6
4RuBpin	2.252	1.745	1.324	50.7	35.6	93.4
1RuBcat	2.135	1.777	1.359	56.0	39.1	84.9
2RuBcat	2.198(2.189)[a]	1.791(1.789)	1.354(1.351)	54.5(54.7)	38.2(38.1)	87.3(87.2)
3RuBcat	2.231	1.752	1.320	51.6	36.3	92.1
4RuBcat	2.208	1.740	1.325	52.4	36.9	90.7
5RuBpin	2.159	1.686	1.394	51.3	40.2	88.5

[a] Optimized geometry at DFT/BP86/TZ2P [63].

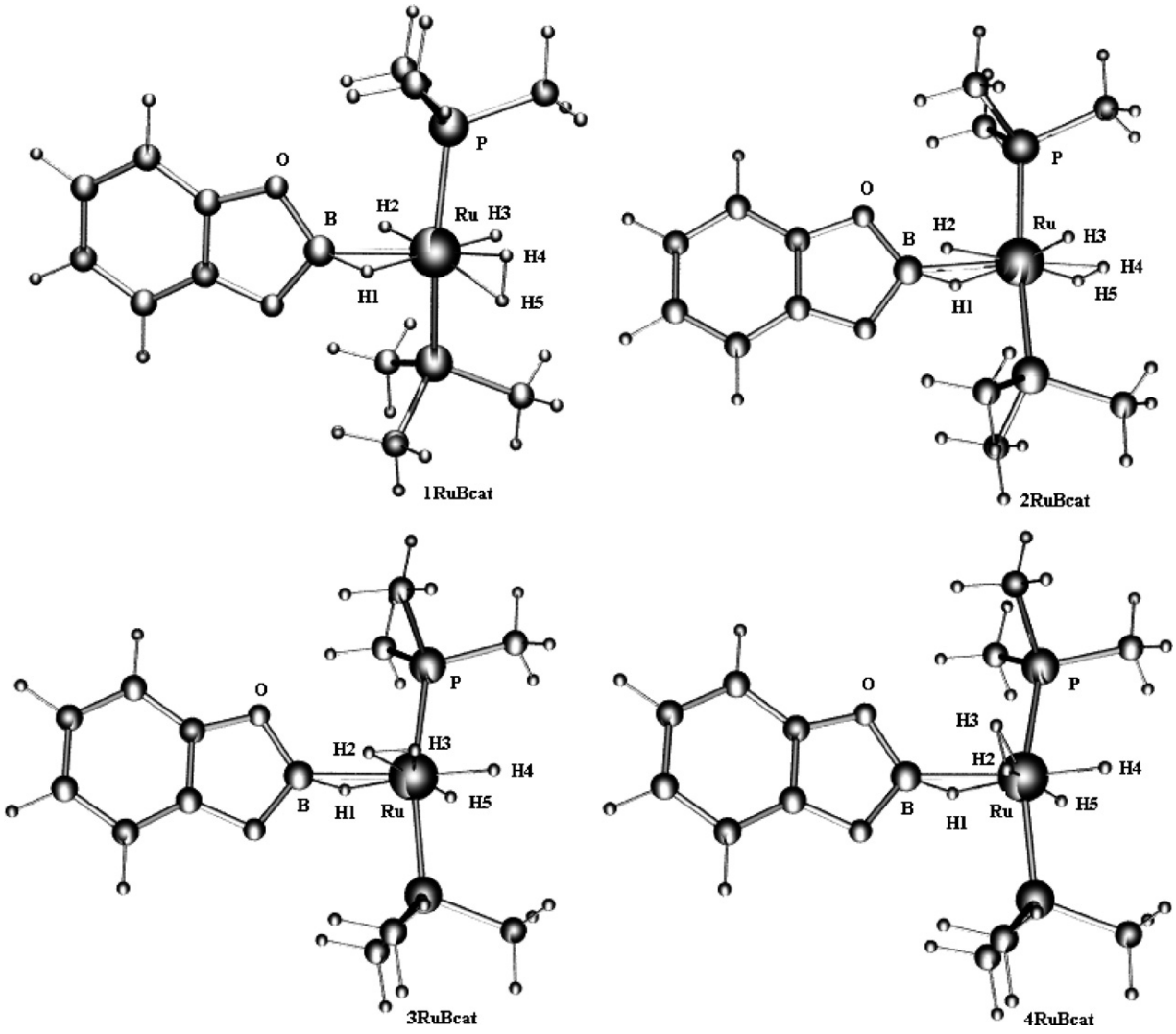

Fig. 5. Optimized geometries of four isomers of $[RuH_2(\eta^2\text{-HBcat})(\eta^2\text{-}H_2)(PCy_3)_2]$.

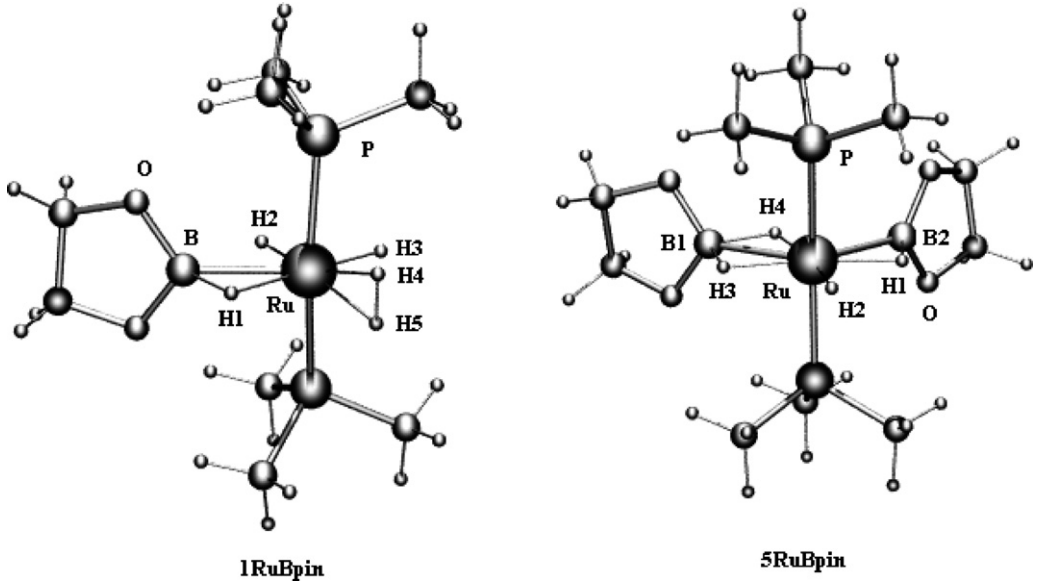

Fig. 6. Calculated geometries of **1RuBpin**, and **5RuBpin**.

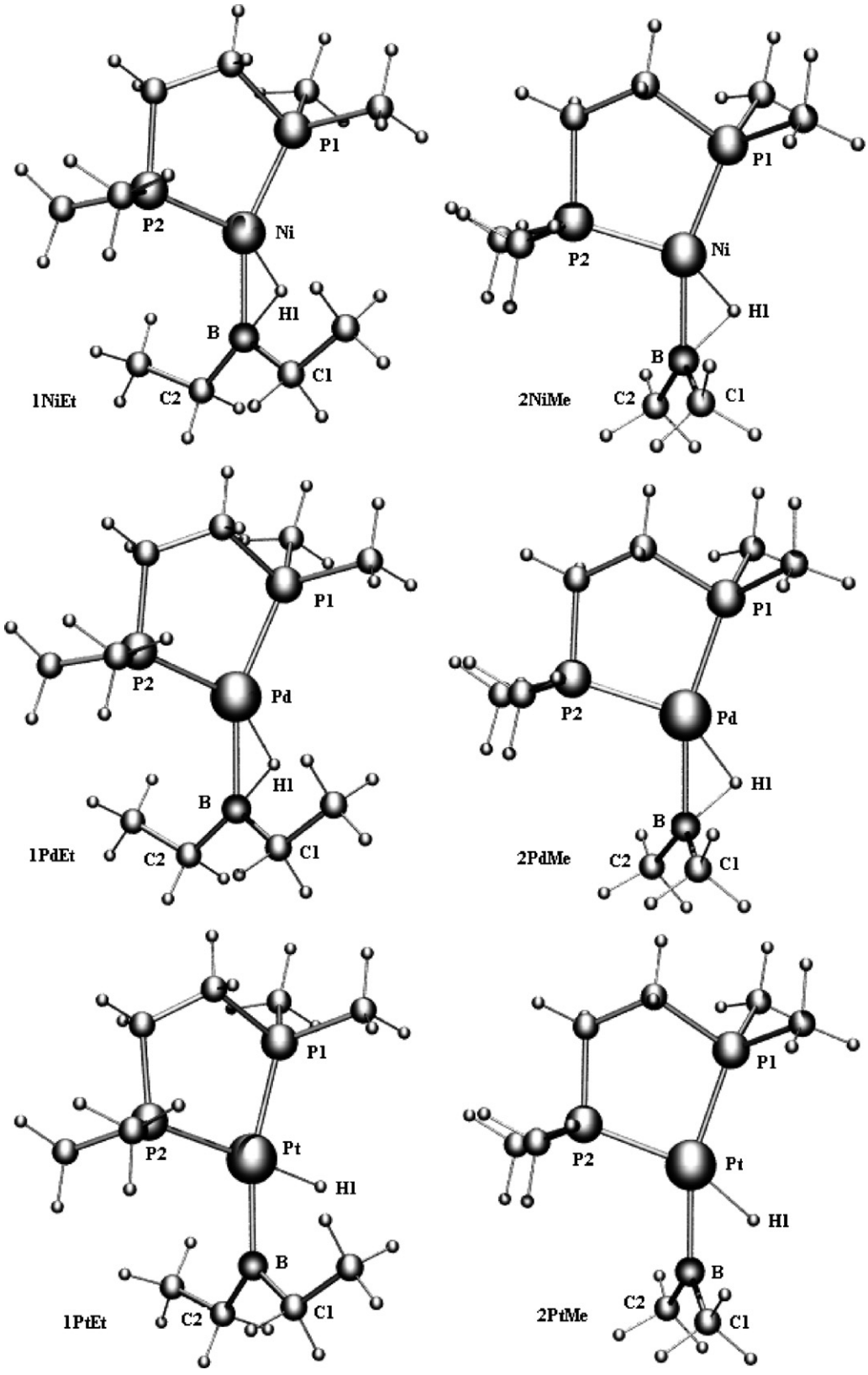

Fig. 7. Calculated geometries of **1NiEt**, **2NiMe**, **1PdEt**, **2PdMe**, **1PtEt** and **2PtMe** at BP86/TZ2P.

Table 10
Selected optimized geometrical parameters for σ-borane complexes $[(Me_2PCH_2CH_2PMe_2)M(\eta^2\text{-}HBR_2)]$[a] at BP86/TZ2P

	1NiEt		**2NiMe**	**1PdEt**	**2PdMe**	$[HBEt_2]$	$[HBMe_2]$
	BP86	BP86[a]	BP86	BP86	BP86	BP86	BP86
Bond distances							
M–B	1.993	2.031	1.964	2.179	2.157		
M–H1	1.575	1.574	1.594	1.751	1.787		
M–P1	2.175	2.221	2.159	2.373	2.159		
M–P2	2.106	2.170	2.092	2.268	2.092		
B–H1	1.370	1.362	1.353	1.355	1.333	1.212	1.208
B–C1	1.604	1.608	1.605	1.596	1.598	1.568	1.567
B–C2	1.597	1.601	1.588	1.592	1.588	1.568	1.567
Bond angles							
M–H1–B	84.9	87.2	83.1	88.1	86.2		
M–B–H1	51.9	50.7	53.7	53.4	55.7		
B–M–H1	43.2	42.1	43.2	38.4	38.1		
P1–M–P2	92.6	92.3	93.4	89.1	89.7		
P1–M–B	154.3	148.9	158.8	156.1	161.2		
P2–M–B	112.4	118.7	107.6	113.8	108.9		
H1–M–P1	115.1	110.3	118.3	121.0	125.1		
C1–B–C2	114.6	111.7	118.5	116.4	118.4	122.5	122.2

Distances are in Å and angles in degrees.
[a] Optimized geometry of $[(Cy_2PCH_2CH_2PCy_2)Ni(HBEt_2)]$.

of theory adopted for the title complexes. On going from nickel to palladium, we observe an increase of the M–B bond distances 1.993 Å in 1NiEt, 1.964 Å in 2NiMe, 2.179 Å in 1PdEt and 2.159 Å in 2PdMe. The Pd–B bond distances in σ-borane complexes 1PdEt and 2PdMe, are longer than the Pd–B bond distances in boryl complex, 2.077(6) Å in $[Pd(Me_2PCH_2CH_2PMe_2)(SnCl_3)\{B\text{-}1,2\text{-}(NMe_2CH_2CH_2)}$ [46,84]. The B–H bond distances 1.370 Å in 1NiEt, 1.353 Å in 2NiMe, 1.355 Å in 1PdEt and 1.333 Å in 2PdMe are longer than expected for a single bond based on covalent radius predictions (1.19 Å) [81] and those obtained by theoretical study for the free borane ligands (1.212 Å in $HBEt_2$, 1.208 Å in $HBMe_2$). The optimized B–H bond distances in σ-borane complexes correspond to a covalent bond order of about 1/2 [82]. The (η^2-B-H) coordination is confirmed by a significant lengthening of the B–H bonds. The B–M–H1 bond angles in the complexes $[(Me_2PCH_2CH_2PMe_2)M(\eta^2\text{-}HBR_2)]$: 43.2° in 1NiEt, 43.2° in 2NiMe, 38.4° in 1PdEt and 38.1° in 2PdMe are very small and are consistent with B–H bonding. These results are consistent with $[(Me_2PCH_2CH_2PMe_2)Ni(HBR_2)]$ and $[(Me_2PCH_2CH_2PMe_2)Pd(HBR_2)]$ being Ni(0) and Pd(0) complexes in which both hydrogen and boron of the $[HBR_2]$ ligands have a bonding interaction with the metal, while preserving B–H bond character. Thus the complexes $[((Me_2PCH_2CH_2PMe_2)Ni(HBR_2)]$ and $[(Me_2PCH_2CH_2PMe_2)Pd(HBR_2)]$ are σ-borane complexes rather than hydride–boryl complexes. On substitution of methyl group for ethyl group, shortening of M–B and B–H bond distances and lengthening of M–H1 bonds distances is observed. It can be inferred from these data that substitution of a methyl group on the boron stabilizes the σ-borane bonding relatively more than the ethyl group. The M–P bond distances trans to the boryl ligand are longer than the M–P bond distances trans to H1 (Table 10).

Some differences of the optimized geometries of $[(Me_2PCH_2CH_2PMe_2)Ni(HBR_2)]$ from the X-ray diffraction data for $[(Cy_2PCH_2CH_2PCy_2)Ni(HBEt_2)]$ by Garcia and co-workers [29] are noted. Can such differences be attributed to the use of dmpe in the model structure instead of dcype in the isolated complex? The optimized geometry of the isolated complex $[(Cy_2PCH_2CH_2PCy_2)Ni(HBEt_2)Ni(HBEt_2)]$ is presented in Fig. 8. The optimized geometrical data, in particular bond angles (Table 10) differ from the X-ray diffraction data and are almost similar with optimized geometries of model complexes $[(Me_2PCH_2CH_2PMe_2)Ni(HBR_2)]$. The B–H bond in

Table 11
Selected optimized geometrical parameters for platinum complexes $[(dmpe)PtH(BR_2)]$ (**1PtEt**, R = Et; **2PtMe**, R = Me) at BP86/TZ2P

	1PtEt	**2PtMe**
Bond distances (Å)		
Pt–B	2.082	2.084
Pt–H1	1.638	1.703
Pt–P1	2.358	2.367
Pt–P2	2.287	2.234
B–H1	2.213	1.611
B–C1	1.597	1.601
B–C2	1.593	1.593
Bond angles (°)		
Pt–H1–B	63.4	77.9
Pt–B–H1	44.7	53.0
B–Pt–H1	71.9	49.1
P1–Pt–P2	86.0	87.0
P1–Pt–B	166.0	161.1
P2–Pt–B	106.6	111.2
H1–Pt–P1	95.7	113.2
C1–B–C2	113.5	116.2
Pt–B–C1	121.0	117.8
Pt–B–C2	125.3	125.7

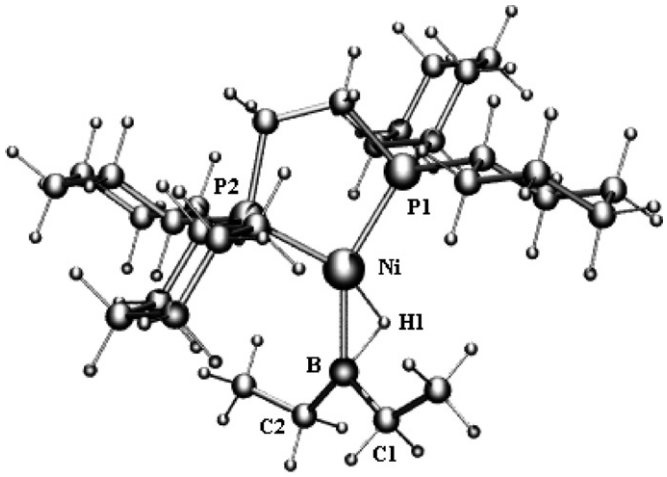

Fig. 8. Calculated geometries of $[(Cy_2PCH_2CH_2PCy_2]Ni(HBEt_2)]$ at BP86/TZ2P.

isolated complex $[(Cy_2PCH_2CH_2PCy_2)Ni(HBEt_2)Ni(HBEt_2)]$ is almost similar to the B–H bond in free $HBEt_2$.

The Pt–B bond distances 2.082 Å in **1PtEt** and 2.084 Å in **2PtMe** (Table 11) are shorter than that expected for a single bond based on covalent radius predictions (2.16 Å) and are in good agreement with experimental results of platinum boryl complexes (Pt–B = 2.03–2.10 Å) 46]. The Pt–H bond distance 1.638 Å in **1PtEt** is almost equal to that expected for a single bond based on covalent radius predictions (1.64 Å). We note the lengthening of the Pt–H bond distance 1.702 Å in **2PtMe**. The B–H bond distances 2.213 Å in **1PtEt** and 1.614 Å in **2PtMe** are much are longer than expected for a single bond based on covalent radius predictions (1.19 Å) [81] and those obtained by theoretical study for the free borane ligands (1.212 Å in $HBEt_2$, 1.208 Å in $HBMe_2$) and correspond to a covalent bond order of 0.04 in **1PtEt** and 0.25 in **2PtMe** [82]. The B–Pt–H1 bond angle 49.2° in **2PtMe** is more acute than 71.9° in 1PtEt, which may, therefore an indication of some H–B interaction. The results of the theoretical investigation suggest that the complex **1PtEt** is a platinum hydride–boryl complex rather than σ-borane complex, while complex **2PtMe** with some residual B–H interaction, is an example of elongated σ-borane complex.

The results of energy decomposition analysis for the complexes **1NiEt**, **1PdEt**, **1PtEt**, **2NiMe**, **2PdMe** and **2PtMe** are presented in Table 12. The calculated bonding energies are **1NiEt** (−33.9 kcal/mol), **1PdEt** (−22.4 kcal/mol), **2NiMe** (−37.7 kcal/mol) and **2PdMe** (−24.1 kcal/mol). There are no experimental M–HBR_2 bond energy data available for $[(Me_2PCH_2CH_2PMe_2)M(HBR_2)]$. The values of nickel complexes are larger and of palladium complexes are smaller than the experimental estimate of 25 ± 3 kcal/mol in $[(\eta^5\text{-}MeC_5H_5)Mn(CO)_2(\eta^2\text{-}HBcat)]$ [24]. We find that the bond dissociation energy in nickel and palladium complexes is greater for the methyl substituents on boron M-(η^2-$HBMe_2$) than the ethyl substituents on boron (η^2-$HBEt_2$). The values of interaction energy, ΔE_{int} as well as orbital interactions ΔE_{orb} decrease on going from nickel to palladium. This was partly due to the fact that the Pd–B and Pd–H bond distances were longer than the Ni–B and Ni–H bond distances, but the nature and properties of the HOMO and LUMO orbitals of the metal fragments and borane fragments also play a role in explaining the orbital interaction differences. The HOMO of $[(Me_2PCH_2CH_2PMe_2)Pd]$ fragment is lower in energy and LUMO is higher in energy than in $[(Me_2PCH_2CH_2PMe_2)Ni]$ fragment. As a result, the LUMO of the metal fragment comes closer in energy to the HOMO of the HBR_2 moiety, allowing for a better donation and a relatively stronger σ-bond interaction in nickel complexes. Similarly, the energy of the HOMO of the $[(Me_2PCH_2CH_2PMe_2)Pd]$ fragment is lowered, which in turn increases the energy gap between the orbitals involved in back donation and leads to a decrease of the π-bond strength in palladium complexes as compared to nickel complexes.

For M-η^2-H-BR_2 (M = Ni, Pd) bonds in the complexes **1NiEt**, **1PdEt**, **2NiMe** and **2PdMe**, the contribution of electrostatic attractions ΔE_{elstat} are greater than the orbital interactions, ΔE_{orb}. The repulsive terms ΔE_{Pauli} were larger in each case. All four complexes **1NiEt**, **1PdEt**, **2NiMe** and **2PdMe** exhibit about 40–44% covalent bonding of the borane ligand to the metal fragment. Studies of chemical bonding using the energy decomposition analysis have indicated that the electron density distribution along bond axes should be taken into account for the interpretation of electrostatic interaction results [85,86]. The reason for the large electrostatic interaction is the anisotropic charge distribution at the metal atom of $[(Me_2PCH_2CH_2PMe_2)M]$ and $[HBR_2]$ fragments. The HOMO of the $[(Me_2PCH_2CH_2PMe_2)M]$ fragments consist primarily of

Table 12
Energy decomposition analysis of $[(Me_2PCH_2CH_2PMe_2)M((HBR_2)]$ (**1NiEt**, **1PdEt**, **1PtEt**, **2NiMe**, **2PdMe**, **2PtMe**) at BP86/TZ2P[a]

	1NiEt	1PdEt	1PtEt	2NiMe	2PdMe	2PtMe
ΔE_{int}	−60.0	−42.8	−132.5	−57.8	−40.0	−88.9
ΔE_{Pauli}	117.6	120.2	308.5	118.9	115.0	222.0
ΔE_{elstat}	−98.7	−98.9	−295.2	−98.5	−92.4	−193.5
ΔE_{orb}[b]	−78.9 (44.4%)	−64.1 (39.3%)	−145.6 (33.0%)	−78.2 (44.3%)	−62.6 (40.4%)	−117.4 (37.8%)
ΔE_{prep}	26.1	20.4	94.8	20.6	15.9	52.3
$\Delta E(-D_e)$	−33.9	−22.4	−37.7	−37.2	−24.1	−36.6

[a] Energy contributions in kcal/mol.
[b] The values in parentheses are the percentage contribution to the total attractive interactions reflecting the covalent character of the bond.

metal d-type functions which is directed toward H and B atoms of borane ligand as well as the anisotropic charge distribution at the H and B atoms in [HBR_2] fragment directed toward metal atom of [$(Me_2PCH_2CH_2PMe_2)M$] fragment. These characteristics should allow for more significant overlap between the electron density on a given fragment and nucleus in the opposite fragment, thus leading to stronger attractive electrostatic interactions.

For the platinum complexes **1PtEt** and **2PtMe**, the preparation energy, ΔE_{prep} as well as interaction energy, ΔE_{int} and its components, ΔE_{Pauli}, ΔE_{elstat}, and ΔE_{orb} are large, since the HBR_2 unit near the dissociation limit. These values are relatively much smaller for **2PtMe** than the **1PtEt** and are greater than those for **1NiEt**, **1PdEt**, **2NiMe** and **2PdMe**. The complex **2PtMe** is intermediate between σ-borane complexes, **1NiEt**, **1PdEt**, **2NiMe** and **2PdMe** and hydride boryl complex **1PtEt**.

7.7. Bonding in rhodium–σ-borane complexes

Fig. 9 shows the optimized geometries of the elongated rhodium–σ-borane complexes [$(\eta^5$-$C_5H_5)Rh(HBpin)_2$] **1Rh** and [$(\eta^5$-$C_5H_5)Rh(HBpin)(Bpin)_2$] **2Rh**. The optimized bond lengths and angles at BP86 are presented in Table 13 [65]. The optimized geometries of the heavy atoms of **1Rh** and **2Rh** closely resemble that found by X-ray diffraction for [$(\eta^5$-$C_5Me_5)Rh(HBpin)_2$] and [$(\eta^5$-$C_5Me_5)Rh(HBpin)(Bpin)_2$] [31]. The optimized structure of **1Rh** which contains almost similar HBpin ligands, differs from the optimized geometry of [$(\eta^5$-$C_5H_5)Rh(HBO_2C_2H_4)_2$] [31]. The Rh–B bond distances 2.054 and 2.067 Å in **1Rh** and 2.074, 2.065, 2.083 Å, **2Rh** are slightly shorter than that expected for single bond based on covalent radius predictions (2.09 Å) [57]. The Rh–H1, 1.583 Å and Rh-H2, 1.585 Å bond distances are equal. The B–H bond distances B1–H1, 1.696 and 1.747 Å in **1Rh** and 1.686 Å in **2Rh** are longer than expected for a single bond based on covalent radius predictions (1.19 Å) and those obtained by theoretical study for the free borane ligands (1.190 Å in HBpin). The B1–Rh–H1 bond angles 55.6° and 52.6° in 1Rh and 2Rh respectively and B2–Rh–H2 bond angle in 1Rh are larger than the B–M–H bond angles in σ-borane complexes (37°–41°) [28,41,42] and are consistent with rhodium–σ-borane bonding, preserving some B–H bond character.

Table 14 gives the Wiberg bond indices [83] (WBI), which provide bond orders, and the natural bond orbital (NBO) analysis. The WBI values of the Rh–B bonds of the complexes **1Rh** and **2Rh** are small ∼0.45. The B–H bond orders: $W_{B1–H1}$ 0.33 in 1Rh, 0.31 in 2Rh and $W_{B2–H2}$ 0.31 in 1Rh are reduced by ∼1/3 ($W_{B–H}$ 0.96 in free HBpin ligand). The computed charges indicate that the rhodium atom and cyclopentadienyl group always carries a negative charge, while H atom and HBpin are positively charged.

A more definitive picture of Rh–B, Rh–H and B–H bonding can be obtained through NBO analysis of the delocalized Kohn–Sham orbitals. The characteristics of the Rh–B and Rh–H bonding orbitals are listed in Table 13. The occupancies of these orbitals are relatively low. The Rh–B and Rh–H bonding orbitals are strongly polarized towards rhodium. A better explanation for the difference in B–H bond distances in manganese–σ-borane complex and stretched rhodium–σ-borane complexes **1Rh** and **2Rh** can be found by looking at the values of the percentage s-character of the boron along Rh–B, B–O and B–H bonds. The values of the percentage s-character of the B1 atom in **1Rh** are

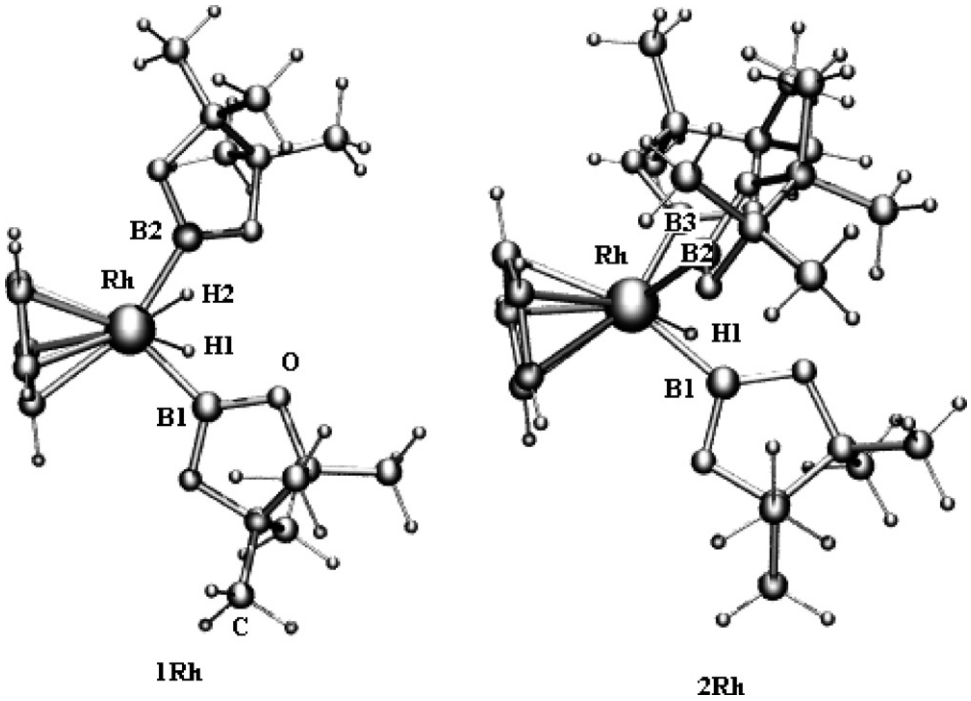

Fig. 9. Optimized geometries of [η^5-$C_5H_5)Rh(H)_2(Bpin)_2$] **1Rh** and [η^5-$C_5H_5)RhH(Bpin)_3$] **2Rh** at BP86/TZ2P.

Table 13
Selected optimized geometrical parameters for stretched rhodium–σ-borane complexes [(η^5-C_5H_5)Rh(HBpin)$_2$] **1Rh**, [(η^5-C_5H_5)Rh(HBpin)(Bpin)$_2$] **2Rh** at BP86/TZ2P and X-ray data for **(24)**[a] and **(25)**[a]

	[(η^5-C_5H_5)Rh(HBpin)$_2$]		[(η^5-C_5H_5)Rh(HBpin)(Bpin)$_2$]	
	BP86	X-ray[a]	BP86	X-ray[a]
Bond distances				
Rh–B1	2.054	2.055(7)	2.074	2.059(3)
Rh–B2	2.067	2.081(6)	2.065	2.059(3)
Rh–B3			2.083	2.071(3)
Rh–H1	1.583	1.47(6)	1.580	1.47(3)
Rh–H2	1.585	1.59(6)		
B1–H1	1.696	1.65(4)	1.686	1.69(3)
B2–H2	1.747	1.70(6)		
B1–H2	2.280	2.30(6)	2.037	
B2–H1	2.231	2.21(6)	2.897	
B3–H1				
Bond angles				
B1–Rh–B2	104.4	104.0(2)	104.0	103.40(12)
B1–Rh–B3			74.3	73.16(12)
B2–Rh–B3			81.0	80.34(13)
H1–Rh–H2	93.9	81(3)		
H1–Rh–B1	55.6	53.1(17)	52.6	54.3(10)
Rh–H1–B1	76.0		78.8	
Rh–B1–H1	48.4		48.3	
H1–Rh–B2	76.0	75.6(17)	66.2	66.4(10)
Rh–H1–B2	61.6		68.3	
Rh–B2–H1	42.4		45.3	
H2–Rh–B2	53.4	53(2)		
Rh–H2–B2	78.0			
Rh–B2–H2	48.6			
H2–Rh–B1	74.4	73(2)		
Rh–H2–B1	62.5			
Rh–B1–H2	43.2			
H1–Rh–B3		103.7		104.9(11)
Rh–H1–B3	44.3			
Rh–B3–H1	32.0			

Distances are in Å and angles in degrees.
[a] X-ray data for [(η^5-C_5Me_5)Rh(HBpin)$_2$] **(24)** and [(η^5-C_5Me_5)Rh(HBpin)(Bpin)$_2$] **(25)** are taken from ref. [31].

Table 14
Wiberg bond indices, and results of the NBO analysis [BP86/TZ2P] in stretched rhodium–σ-borane complexes [(η^5-C_5H_5)Rh(HBpin)$_2$] **1Rh** and [(η^5-C_5H_5)Rh(HBpin)(Bpin)$_2$] **2Rh**

	[(η^5-C_5H_5)Rh(HBpin)$_2$]	[(η^5-C_5H_5)Rh(HBpin)(Bpin)$_2$]
Wiberg bond indices		
Rh–B1	0.49	0.44
Rh–B2	0.50	0.53
Rh–B3		0.50
Rh–H1	0.38	0.35
Rh–H2	0.40	
B1–H1	0.33	0.31
B2–H2	0.31	
NBO charges		
Rh	−0.03	−0.07
H1	0.10	0.12
H2	0.10	
Cp	−0.23	−0.21
Bpin(B1)	0.03	0.07
Bpin(B2)	0.03	0.03
Bpin(B3)		0.04

	[(η^5-C_5H_5)Rh(HBpin)$_2$]		[(η^5-C_5H_5)Rh(HBpin)(Bpin)$_2$]		
Rh–B Bond	Rh–B1 (1.71)[a]	Rh–B2 (1.73)[a]	Rh–B1 (1.63)[a]	Rh–B2 (1.80)[a]	Rh–B3 (1.79)[a]
NBO analysis					
Rh					
%	66.8	66.9	66.4	68.1	67.7
%s	29.8	28.5	32.2	22.8	20.1
%p	0.0	0.0	0.0	0.0	0.0
%d	70.2	71.5	67.8	77.2	79.9
%f	0.0	0.0	0.0	0.0	0.0
B					
%	33.2	33.1	33.6	31.9	32.3
%s	38.1	37.9	38.6	37.4	38.5
%p	61.6	61.8	61.1	62.4	61.3
%d	0.3	0.3	0.3	0.2	0.2

	[(η^5-C_5H_5)Rh(HBpin)$_2$]		[(η^5-C_5H_5)Rh(HBpin)(Bpin)$_2$]
Rh–H bond	Rh–H1 (1.71)[a]	Rh–H2 (1.74)[a]	Rh–H1 (1.67)[a]
Rh			
%	64.6	64.6	65.4
%s	20.9	19.9	24.2
%p	0.0	0.0	0.0
%d	79.1	80.0	75.8
%f	0.0	0.0	0.0
H			
%	35.4	35.4	34.6
%s	100.0	100.0	100.0

[a] Occupancy.

38.1% along Rh–B1 bond, 32.0% and 29.7% along B1–O bonds. These results reveal that in **1Rh** complex pure 2p orbital of boron interacts with s orbital of hydrogen atoms H1 and H2 of the borane ligands. In contrast, for manganese–σ-borane complex [(η^5-MeC_5H_4)Mn(CO)$_2$(HBpin)] [41], the hybrid orbital of boron along B–H bond contains 20.4% s character and 79.3% p-character. This is one of the reasons why the B–H bond is longer in stretched σ-borane rhodium complexes. We now compare bonding between Rh-Bpin and Rh-(HBpin) bonds in **2Rh** complex. Table 14 shows that less 2s character and more 2p character goes to the Rh–B2 and Rh–B3 bonds of boryl ligand than to the Rh–B1 bond of the borane ligand.

7.8. Bonding in intermediate iron and tungsten–σ-borane complexes

Intermediate σ-borane complexes [(η^5-C_5H_5)Fe(CH_3)(CO)(HB(OCH_2)$_2$)] **(29)**, **(30)** and [(η^5-C_5H_5)W(CH_3)(CO)$_2$(HB(OCH_2)$_2$)] **(31)**, **(32)** have been proposed in the reaction of [(η^5-C_5H_5)M(CH_3)(CO)$_n$(HB(OCH_2)$_2$)] with alkane [40]. Calculated bond distances at BP86 level: for **(29)**, Fe–H 1.57 Å, Fe–B 2.11 Å and B–H, 1.31 Å; for **(30)**, Fe–H 1.54 Å, Fe–B 2.09 Å and B–H, 1.33 Å; for **(31)**, W–H 1.78 Å, W–B 2.42 Å and B–H, 1.33 Å and for **(32)** W–H 1.80 Å, Fe–B 2.47 Å and B–H, 1.29 Å are consistent with the σ-borane complexes.

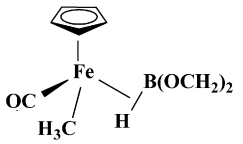

(29)

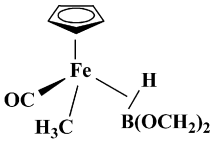

(30)

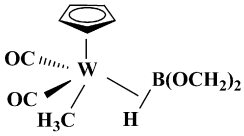

(31)

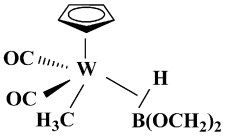

(32)

8. Conclusion

Synthesis, structure and bonding in transition metal–σ-borane complexes have attracted much attention in the last few years and it may be expected that further progress will be made in the future. The review summarizes the synthesis, spectral studies and progress in the understanding of the nature of the metal–σ-borane bonds, which has been gained in recent theoretical studies. Geometrical data (both experimental and theoretically calculated) show M–B, M–H and B–H bond distances longer than the sum of covalent radii. These results are consistent with the interaction of both boron and hydrogen with the central metal, while preserving the B–H bond character. The nature of the metal–borane interactions is quantitatively analyzed with an energy decomposition analysis. The $[L_nM]$–$[\eta^2$-$BHR_2]$ bonding in metal–borane complexes is more than half electrostatic.

Acknowledgement

I thank Prof. Gernot Frenking, Fachbereich Chemie, Philipps University Marburg for useful comments on borane complexes of manganese and rhenium.

References

[1] (a) G.J. Kubas, in: J.P. Fackler (Ed.), Metal Dihydrogen and σ-Bond Complexes, Kluwer Academic/Plenum Publishers, New York, 2001;
(b) G.J. Kubas, Catal. Lett. 105 (2005) 79.
[2] G.J. Kubas, R.R. Ryan, B.L. Swanson, P.J. Vergamini, H.J. Wasserman, J. Am. Chem. Soc. 106 (1984) 451.
[3] G.J. Kubas, Acc. Chem. Res. 21 (1988) 120.
[4] R.H. Crabtree, Acc. Chem. Res. 23 (1990) 95.
[5] P.G. Jessop, R.H. Morris, Coord. Chem. Rev. 121 (1992) 155.
[6] D.M. Heinekey, W.J. Oldham Jr., Chem. Rev. 93 (1993) 913.
[7] R.H. Crabtree, Angew. Chem. Int. Ed. Engl. 32 (1993) 789.
[8] M.A. Esteruelas, L.A. Oro, Chem. Rev. 98 (1998) 577.
[9] J. Tomas, A. Lledós, Y. Jean, Organometallics 17 (1998) 190.
[10] G. Frenking, N. Fröhlich, Chem. Rev. 100 (2000) 717.
[11] F. Maseras, A. Lledós, E. Clot, O. Eisenstein, Chem. Rev. 100 (2000) 601.
[12] U. Schubert, Adv. Organomet. Chem. 30 (1990) 151.
[13] J.Y. Corey, M. Elder, J. Braddock-Wilking, Chem. Rev. 99 (1999) 175.
[14] S. Sabo-Etienne, B. Chaudret, B. Coord, Chem. Rev. 178 (1998) 381.
[15] F. Delpech, S. Sabo-Etienne, J.-C. Daran, B. Daran, B. Chaudret, K. Hussein, C.J. Marsden, J.-C. Barthelat, J. Am. Chem. Soc. 121 (1999) 6668.
[16] I. Atheaux, B. Donnadieu, V. Rodriguez, S. Sabo-Etienne, B. Chaudret, K. Hussein, J.-C. Barthelat, J. Am. Chem. Soc. 122 (2000) 5664.
[17] N.M. Yardy, F.R. Lemke, L. Brammer, Organometallics 20 (2001) 5670.
[18] G.I. Nikonov, Organometallics 22 (2003) 1597.
[19] D.I. Lichtenberger, Organometallics 22 (2003) 1599.
[20] (a) S.R. Dubberley, S.K. Ignatov, N.H. Rees, A.G. Razuvaev, P. Mountford, G.I. Nikonov, J. Am. Chem. Soc. 125 (2003) 642;
(b) G.I. Nikonov, Adv. Organomet. Chem. 53 (2005) 217 (and references therein).
[21] J.F. Hartwig, C.N. Muhoro, X. He, O. Eisenstein, R. Bosque, F. Maseras, J. Am. Chem. Soc. 118 (1996) 10936.
[22] C.N. Muhoro, J.F. Hartwig, Angew. Chem, Int. Ed. Engl. 36 (1997) 1510.
[23] C.N. Muhoro, X. He, J.F. Hartwig, J. Am. Chem. Soc. 121 (1999) 5033.
[24] S. Schlecht, J.F. Hartwig, J. Am. Chem. Soc. 122 (2000) 9435.
[25] R. Macias, N.P. Rath, L. Barton, Angew. Chem. Int. Ed. 38 (1999) 162.
[26] M. Shimoi, S. Nagai, M. Ichikawa, Y. Kawano, K. Katoh, M. Uruichi, H. Ogino, J. Am. Chem. Soc. 121 (1999) 11704.
[27] V. Montiel-Palma, M. Lumbierres, B. Donnadieu, S. Sabo-Etienne, B. Chaudret, J. Am. Chem. Soc. 124 (2002) 5624.
[28] S. Lachaize, K. Essalah, V. Montiel-Palma, L. Vendier, B. Chaudret, J.-C. Barthelat, S. Saba-Etienne, Organometallics 24 (2005) 2935.
[29] M.G. Crestani, M. Munoz-Hemandez, A. Arevalo, A. Acosta-Ramirez, J. Garcia, J. Am. Chem. Soc. 127 (2005) 18066.
[30] K.S. Cook, C.D. Incarvito, C.E. Webster, Y. Fin, M.B. Hall, J.F. Hartwig, Angew. Chem. Int. Ed. 43 (2004) 5474.
[31] J.F. Hartwig, K.S. Cook, M. Hapke, C.D. Incarvito, Y. Fan, C.E. Webster, M.B. Hall, J. Am. Chem. Soc. 127 (2005) 2538.
[32] W.H. Lam, S. Shimada, A.S. Batsanov, Z. Lin, T.B. Marder, J.A. Cowan, J.A.K. HcMason, G.J. McIntyre, Organometallics 22 (2003) 4557.
[33] C. Widauer, H. Gruetzmacher, T. Ziegler, Organometallics 19 (2000) 2097.
[34] J.F. Hartwig, S.R. Ge Gala, J. Am. Chem. Soc. 116 (1994) 3661.
[35] (a) D.R. Lantero, D.H. Motry, D.L. Ward, M.R. Smith III, J. Am. Chem. Soc. 116 (1994) 10811;
(b) C.N. Iverson, M.R. Smith III, J. Am. Chem. Soc. 121 (1999) 7676.
[36] D.R. Lantero, D.L. Ward, M.R. Smith III, J. Am. Chem. Soc. 119 (1997) 9699.
[37] D.R. Lantero, S.L. Miller, J.Y. Cho, D.L. Ward, M.R. Smith III, Organometallics 18 (1999) 235.
[38] D. Liu, K.C. Lam, Z. Lin, J. Organomet. Chem. 680 (2003) 148.
[39] J.F. Hartwig, C.N. Muhoro, Organometallics 19 (2000) 30.
[40] D. Liu, K.C. Lam, Z. Lin, Organometallics 22 (2003) 2827.
[41] C.E. Webster, Y. Fan, M.B. Hall, J.F. Hartwig, J. Am. Chem. Soc. 125 (2003) 858.
[42] T. Ishiyama, N. Miyaura, J. Organomet. Chem. 680 (2003) 3.
[43] K. Kawamura, J.F. Hartwig, J. Am. Chem. Soc. 123 (2001) 8422.
[44] M. Murata, K. Kawakita, T. Asana, S. Watanabe, Y. Masuda, Bull. Chem. Soc. Jpn. 75 (2002) 825.
[45] C.M. Crudden, D. Edwards, Eur. J. Org. Chem. (2003) 4695.
[46] R.B. Coapes, F.E.S. Souza, R.L. Thomas, J.J. Hall, T.B. Marder, Chem. Commun. (2003) 614.
[47] G.J. Irvine, G. Lesley, T.B. Marder, N.C. Norman, C.R. Rice, E.G. Robins, W.R. Roper, G.R. Whittell, J. Wright, J. Chem. Rev. 98 (1998) 2685.
[48] J.F. Hartwig, K.M. Waltz, C.N. Muhoro, X. He, O. Eisenstein, R. Bosque, F. Maseras, in: W. Siebert (Ed.), Advances in Boron Chemistry, The Royal Society of Chemistry, Cambridge, 1997, p. 373 (Special Publication No. 201).
[49] H. Wadepohl, Angew. Chem. Int. Ed. 36 (1997) 2441.
[50] H. Braunschweig, Angew. Chem. Int. Ed. 37 (1998) 1786.
[51] M.R. Smith III, Prog. Inorg. Chem. 48 (1999) 505.
[52] H. Braunschweig, M. Colling, Coord. Chem. Rev. 223 (2001) 1.
[53] S. Aldridge, D.L. Coombs, Coord. Chem. Rev. 248 (2004) 535.
[54] M.V. Câmpian, J.L. Harris, N. Jasim, R.N. Perutz, T.B. Marder, A.C. Ehitwood, Organometallics 25 (2006) 5093.
[55] J.F. Hartwig, X. He, Angew. Chem. Int. Ed. 35 (1996) 315.
[56] J.F. Hartwig, X. He, Organometallics 15 (1996) 5350.
[57] P.L. Callaghan, R. Fernandez-Pacheco, N. Jasim, S. Lachaize, T.B. Marder, R.N. Perutz, E. Rivalta, S. Sabo-Etienne, Chem. Commun. (2004) 242.
[58] R.N. Perutz, S. Sabo-Etienne, Angew. Chem. Int. Ed. 46 (2007) 2578.
[59] A. Caballero, S. Sabo-Etienne, Organometallics 26 (2007) 1191.
[60] T.J. Marks, J.R. Kolb, Chem. Rev. 77 (1977) 263.

[61] Z. Xu, Z. Lin, Coord. Chem. Rev. 156 (1966) 139.
[62] W.H. Lam, Z. Lin, Organometallics 19 (2000) 5093.
[63] K.K. Pandey, unpublished work.
[64] K.K. Pandey, J. Organomet. Chem. 692 (2007) 1997.
[65] K.K. Pandey, J. Mol. Struct. (Theochem) 807 (2007) 61.
[66] K.K. Pandey, J. Mol. Struc. (Theochem) accepted.
[67] K.K. Pandey, Inorg. Chem. Commun. in press.
[68] K.K. Pandey, Inorg. Chem. 40 (2001) 5092.
[69] A. Antinolo, F. Carrillo-Hermosilla, J. Fernandez-Baeza, S. Garcia-Yuste, A. Otero, M. Rodriguez, J. Sanchez-Prada, E. Villasenor, R. Gelabert, M. Moreno, J.M. Lluch, A. Ledós, Organometallics 19 (2000) 3654.
[70] K. Lammertsma, T. Ohwada, J. Am. Chem. Soc. 118 (1996) 7247.
[71] J.S. Craw, G.B. Bacskay, N.S. Hush, J. Am. Chem. Soc. 116 (1994) 5937.
[72] D.M. Heinekey, A. Ledós, J.M. Lluch, Chem. Soc. Rev. 33 (2004) 175.
[73] D.G. Gusev, J. Am. Chem. Soc. 126 (2004) 14249.
[74] A.D. Becke, Phys. Rev. A 38 (1988) 3098.
[75] J.P. Perdew, Phys. Rev. B 33 (1986) 8822.
[76] (a) C. Chang, M. Pelissier, Ph. Durand, Phys. Scr. 34 (1986) 394;
(b) J.-L. Heully, I. Lindgren, E. Lindroth, S. Lundquist, A.-M. Martensson-Pendrill, J. Phys. B 19 (1986) 2799;
(c) E. van Lenthe, E.J. Baerends, J.G. Snijders, J. Chem. Phys. 99 (1993) 4597;
(d) E. van Lenthe, E.J. Baerends, J.G. Snijders, J. Chem. Phys. 105 (1996) 6505;
(e) E. van Lenthe, R. van Leeuwen, E.J. Baerends, J.G. Snijders, Int. J. Quantum Chem. 57 (1996) 281;
(f) E. van Lenthe, A.E. Ehlers, E.J. Baerends, J. Chem. Phys. 110 (1999) 8943.
[77] J.G. Snijders, E.J. Baerends, P. Vernooijs, At. Data Nucl. Data Tables 26 (1982) 483.
[78] E.J. Baerends, J.A. Autschbach, A. Berces, C. Bo, P.M. Boerrigter, L. Cavallo, D.P. Chong, L. Deng, R.M. Dickson, D.E. Ellis, L. Fan, T.H. Fischer, C. Fonseca Guerra, S.J.A. van Gisbergen, J.A. Groeneveld, O.V. Gritsenko, M. Grüning, F.E. Harris, P. van den Hoek, H. Jacobsen, G. van Kessel, F. Kootstra, E. van Lenthe, V.P Osinga, S. Patchkovskii, P.H.T. Philipsen, D. Post, C.C. Pye, W. Ravenek, P. Ros, P.R.T. Schipper, G. Schreckenbach, J.G. Snijders, M. Sola, M. Swart, D. Swerhone, G. te Velde, P. Vernooijs, L. Versluis, O. Visser, E. Wezenbeek, G. Wiesenekker, S.K. Wolff, T.K. Woo, T. Ziegler, ADF, Scientific Computing & Modelling NV, The Netherlands, 2004.
[79] (a) K. Morokuma, J. Chem. Phys. 55 (1971) 1236;
(b) K. Morokuma, Acc. Chem. Res. 10 (1977) 294.
[80] (a) T. Ziegler, A. Rauk, Theor. Chim. Acta 46 (1977) 1;
(b) T. Ziegler, A. Rauk, Inorg. Chem. 18 (1979) 1558;
(c) T. Ziegler, A. Rauk, Inorg. Chem. 18 (1979) 1755.
[81] (a) A.F. Wells, Structural Inorganic Chemistry, 5th ed., Clarendon, Oxford, 1984;
(b) L. Pauling, The Nature of the Chemical Bond, 3rd ed., Cornell University Press, Ithaca, NY, 1960.
[82] L. Pauling, The Nature of the Chemical Bond, 3rd ed., Cornell University Press, New York, 1960. p. 239: The relationship of bond order to length is given by $dn = d1 – 0.71 \log n$ where n is the bond order, $d1$ and dn are the lengths of bonds with bond order1 and n, respectively.
[83] K.A. Wiberg, Tetrahedron 24 (1968) 1083.
[84] S. Onozawa, Y. Hatanaka, T. Sakakura, S. Shimada, M. Tanaka, Organometallics 15 (1996) 5450.
[85] M. Lein, A. Szabó, A. Kovács, G. Frenking, Faraday Discuss. 124 (2003) 365.
[86] G. Cavigliasso, N. Kaltsoyannis, Inorg. Chem. 46 (2007) 3557.